

LL E Review

Quarterly Report



January, 1982–March, 1982

Laboratory for Laser Energetics
College of Engineering and Applied Science
University of Rochester
250 East River Road
Rochester, New York 14623



LLE Review

Quarterly Report

Editor: S. D. Jacobs
(716-275-4837)

January, 1982–March, 1982

Laboratory for Laser Energetics
College of Engineering and Applied Science
University of Rochester
250 East River Road
Rochester, New York 14623



The work described in this volume includes ongoing research at the Laboratory for Laser Energetics which is supported in part by the Empire State Electric Energy Research Company (ESEERCO), the General Electric Company, the New York State Energy Research and Development Authority (NYSERDA), Northeast Utilities, the Standard Oil Company (Ohio), the University of Rochester, and various governmental agencies, including the Department of Energy, the Air Force Office of Scientific Research, the National Institutes of Health, and the National Science Foundation.

IN BRIEF

This edition of the LLE Review contains articles on new developments in thin film coating research, OMEGA uniformity experiments, plasma theory, and laser fusion target fabrication. Some of the highlights of work described in this issue are as follows:

- Modulated transmission ellipsometry has been used to measure, with spatial resolution of 20 μm , the distribution of anisotropic stress around defects in dielectric thin films. With this technique it will be possible to study the relationship between coating stress and laser-induced damage for coating materials and designs of interest to LLE.
- The performance of ablatively driven laser fusion targets on OMEGA with respect to irradiation uniformity is reported. It has been found that even high aspect ratio shells maintain their integrity when the uniformity is sufficiently good.
- Thermal smoothing of nonuniformities in laser deposition on target was examined using a steady-state ablation model. Saturation of the heat flux is found to reduce the laser intensity required for smoothing substantially below the value previously estimated using only classical transport.
- An experimental investigation of biased sputter deposition shows that improved surface smoothness is produced on target pusher layers. This technique also provides improvements in the microstructure and density uniformity of the pusher layer material.

LLE REVIEW

- An information management system has been established for the Target Fabrication Group on the CYBER 175 computer. This system provides automated data entry and retrieval during the processing and use of OMEGA implosion targets.

CONTENTS

	<i>Page</i>
IN BRIEF	iii
CONTENTS	v
Section 1 LASER SYSTEM REPORT	1
1.A GDL Facility Report	1
1.B OMEGA Facility Report	1
1.C Anisotropic Stress around Defects in Thin Films	3
Section 2 PROGRESS IN LASER FUSION	11
2.A Irradiation Uniformity Experiments on OMEGA	11
2.B Thermal Smoothing of Irradiation Nonuniformities in Laser-Driven Fusion	18
Section 3 DEVELOPMENTS IN MICROFABRICATION	25
3.A Biased Sputtering of Target Pusher Layers	25
3.B An Interactive Information Management Data Base for Fusion Target Fabrication	28
Section 4 NATIONAL LASER USERS FACILITY NEWS	33
PUBLICATIONS AND CONFERENCE PRESENTATIONS	36



Georg Albrecht, LLE staff scientist, is preparing for fine adjustment of a Kuizenga oscillator, part of which is visible in the lower left. In the background are the electronic controls for two of these oscillators.

Section 1

LASER SYSTEM REPORT

1.A GDL Facility Report

The GDL facility continued operations during the second quarter of FY82 in support of the 3ω interaction program, the National Laser Users Facility (NLUF), and the Damage Testing Facility (DTF).

A total of 688 shots were delivered by the facility in the period January 1 to March 31, 1982. The shot distribution was as follows:

3ω Target Experiments	225	Shots
NLUF	141	
DTF	229	
Alignment and Calibration	<u>93</u>	
TOTAL	688	Shots

National Laser Users Facility operations during this time included shots for users from the University of Maryland, UCLA, Yale, NRL, and for the x-ray biophysics group.

1.B OMEGA Facility Report

During the quarter January 1 to March 31, 1982, 432 OMEGA system shots were fired. The principal activity on the system was experimental target shooting. In fact, both the absolute number and the percentage of target shots set new quarterly records.

To accomplish the projected target shot schedule, the Laser Operations Group concentrated on maintaining and firing OMEGA. No significant modifications were attempted and no major failures occurred. On the two scheduled shooting days per week, staggered shift assignments allowed 14–16 hour shooting stints—an effective way to boost the shot rate.

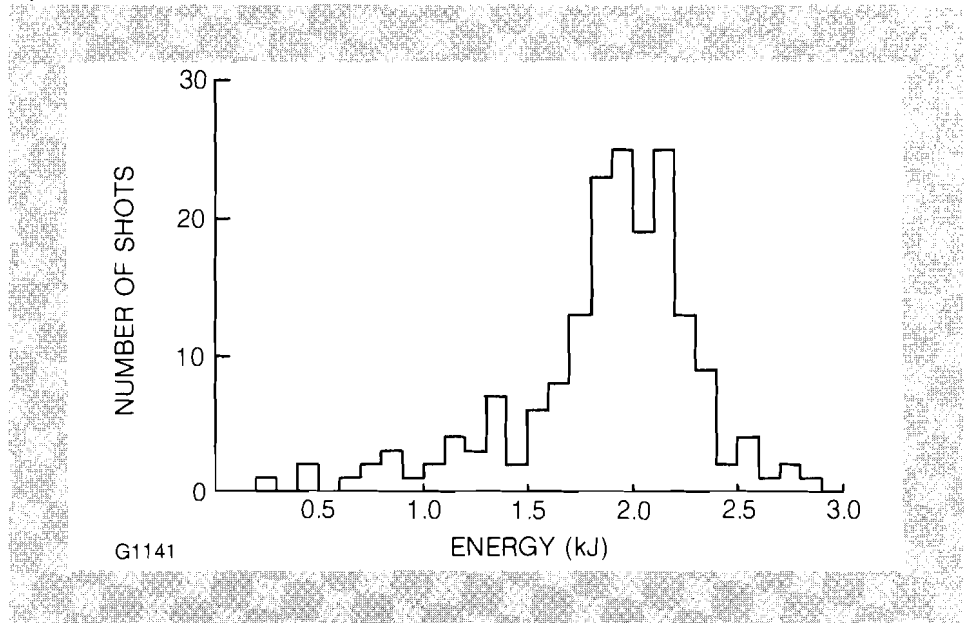
Table 1 is the breakdown by category of the system shots for this quarter. Figure 1 is the shot energy histogram for all the 24-beam shots. The lower energy shots were mostly prescribed in advance. Only 3 of the shots represent system misfires. During the entire period the new 3-meter oscillator was configured for 1 nsec pulses. For all target shots the mean and standard deviation for the pulse duration was $0.963 \text{ nsec} \pm 0.143 \text{ nsec}$.

Table 1
OMEGA laser system shot category distribution January 1 to March 31, 1982.

Beam balance, the ratio of rms fluctuations to mean energy, was $9.3\% \pm 4.2\%$ for all target shots except those with deliberately unbalanced beam energies.

January 1, 1982 - March 31, 1982			
CATEGORY	NUMBER OF SHOTS	PERCENT	
Target Shots	193	45	
Driver Align and Test	122	28	
Beamline c/o and Calibration	49	11	
Software Test and Timing	52	12	
Miscellaneous, Other	16	4	
G1140 TOTAL		432	100

Fig. 1
24-Beam target shots from January 1 to March 31, 1982.



1.C Anisotropic Stress around Defects in Thin Films

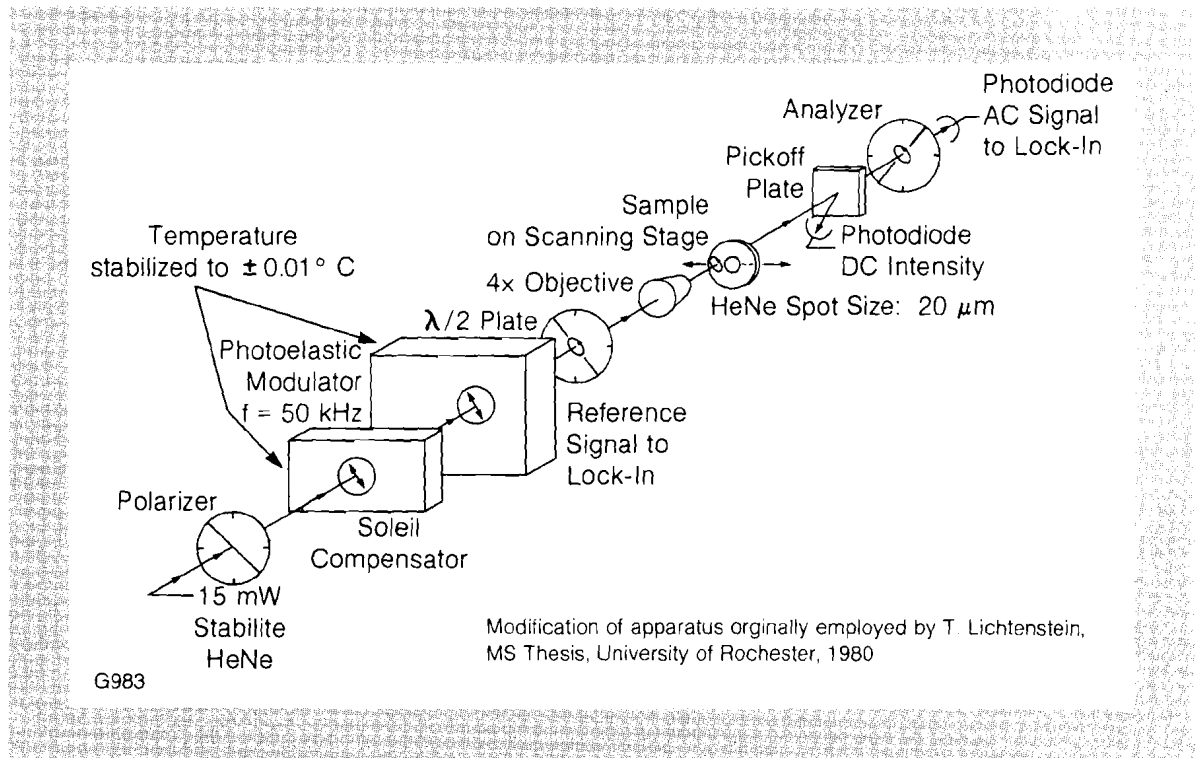
Research at LLE is presently being conducted on laser-induced damage in multilayer dielectric thin film coatings. Through the use of optical microanalytical techniques we hope to eventually understand the nature of coating defects which lower the damage thresholds of thin films. Our laser damage tester was described in LLE Review Volume 7, and the use of photoacoustic absorption spectroscopy for defect characterization was discussed in Volume 9. In this issue we describe a second technique for looking at defects in thin films, which is sensitive only to mechanical stress.

Scientific papers^{1, 2} suggest that there is a correlation between mechanical stress in dielectric multilayer thin films and their laser damage resistance. Work done prior to 1980, however, attempted to investigate the relationship between coating stress and laser damage either indirectly, with calculations based on tabulated data for individual evaporants,¹ or through the use of *spatially averaged* measurements of stress on coated parts with high diameter to thickness aspect ratios.² In 1980, T. Lichtenstein proposed and demonstrated³ that mechanical stress in thin films could be measured using modulated ellipsometry in transmission. Lichtenstein's technique did not require any special coating or substrate geometry and, more importantly, was capable of generating a one-dimensional scan of mechanical stress across a coated substrate with *spatial resolution* approaching $10\ \mu\text{m}$.

Fig. 2

Apparatus for modulated transmission ellipsometry. Optical retardation in a sample is measured with an ac lock-in amplification technique, using a photoelastic modulator (Hinds International, Inc., model PEM-FS4) operating at a frequency of 50 kHz. Optical retardance is directly proportional to stress in the sample.

With instrument modifications we have refined Lichtenstein's technique. Figure 2 shows our modified apparatus. Mechanical stress is



wavelength-independent. We therefore use a stable helium-neon laser as our probe source. A photoelastic modulator, (PEM), operating at a frequency of 50 kHz imparts a sinusoidally varying optical phase retardation of $\pm 158 \text{ nm}$ ($\pm \lambda/4$ at a wavelength of 632.8 nm) to the linearly polarized output of the HeNe. An analyzer converts this phase information to ac intensity and the signal is picked up by a photodiode and displayed on a lock-in amplifier. The lock-in is operated in its high dynamic range mode using an electronic signal from the PEM for reference. A 4X microscope objective focuses the laser beam to a $20 \mu\text{m}$ spot at the sample plane. Samples are moved transverse to the beam in the focal plane of the objective, at a linear scanning rate of 1 mm/minute. A rotatable half waveplate is incorporated into the apparatus to enable the plane of polarization of the HeNe at the sample to be rotated to any arbitrary orientation with respect to the same translation direction. The analyzer is similarly capable of rotation so that it can always be oriented with its pass direction orthogonal to the polarization direction of light incident on the sample.

The apparatus of Fig. 2 measures the optical phase retardation, Γ , introduced to the laser beam by a sample under investigation. Γ is related to the thickness, t , of the sample and optical anisotropy or birefringence, Δn , in the sample as

$$\Gamma(\text{nm}) = t\Delta n \quad (1)$$

The optical phase retardation is directly proportional to the stress, σ , within the sample and can be calculated with a knowledge of sample stress-optic coefficient, c_o , as

$$\sigma(\text{kg/cm}^2) = \Gamma(\text{nm})/c_o \text{ (nm - cm/kg)} t \text{ (cm)} \quad (2)$$

The advantage of measuring stress with modulated transmission ellipsometry is the simplicity of acquiring retardance data. Absolute values of Γ can be obtained provided the apparatus is first calibrated with a Soleil compensator (see Fig. 2). In addition, the sensitivity of the measurement is very high, because it is an ac phase-sensitive technique and because the Soleil compensator can be adjusted to cancel residual birefringence due to all components, other than the sample itself, located between the polarizer and analyzer. Retardance values of 0.01 nm can be measured with excellent repeatability, provided that the Soleil compensator and PEM are temperature stabilized to $\pm 0.1^\circ\text{C}$ or better. For a sample $1 \mu\text{m}$ in thickness, $\Gamma = 0.01 \text{ nm}$ corresponds to an index change of $\Delta n = 0.00001$ and a stress of $\sigma = 50 \text{ kg/cm}^2$ ($c_o = 2 \text{ nm - cm/kg}$). Stresses in thin films extend from $\pm 3000 \text{ kg/cm}^2$ down, and therefore fall easily within the sensitivity capability of the apparatus.

In addition to high sensitivity, modulated transmission ellipsometry can yield spatially resolved retardance (and therefore stress) information with resolution of $20 \mu\text{m}$ or less. The directionality of stress in samples can also be elucidated by manipulating the polarization direction of the probe laser. The one disadvantage to the technique is a lack of discrimination in the longitudinal direction through the sample being

probed. Stress from both the coating and the underlying substrate add together, and only the algebraic sum is measured. Differentiation between coating and substrate stress is sometimes difficult, and will be examined for a number of examples below.

Modulated transmission ellipsometry of thin films works best when the substrate possesses very little residual internal stress. Figure 3 shows the optical retardance commonly observed in 50 mm diameter by 6.35 mm thick BK-7, fused silica, and "Pyrex" substrates used in this work. Because it is a well-annealed optical glass product, BK-7 exhibits a very small amount of residual internal stress, and therefore constitutes an ideal substrate material. Fused silica, when cut into discs from rod stock, exhibits the radially symmetric retardance profile characteristic of annealed rods. The retardance across the part is still smoothly varying, and quite suitable for stress studies. Possibly because of the presence of index inhomogeneities or striae, "Pyrex" exhibits a very irregular or "noisy" retardance profile, making it a less desirable substrate for investigations of stress in thin film coatings.

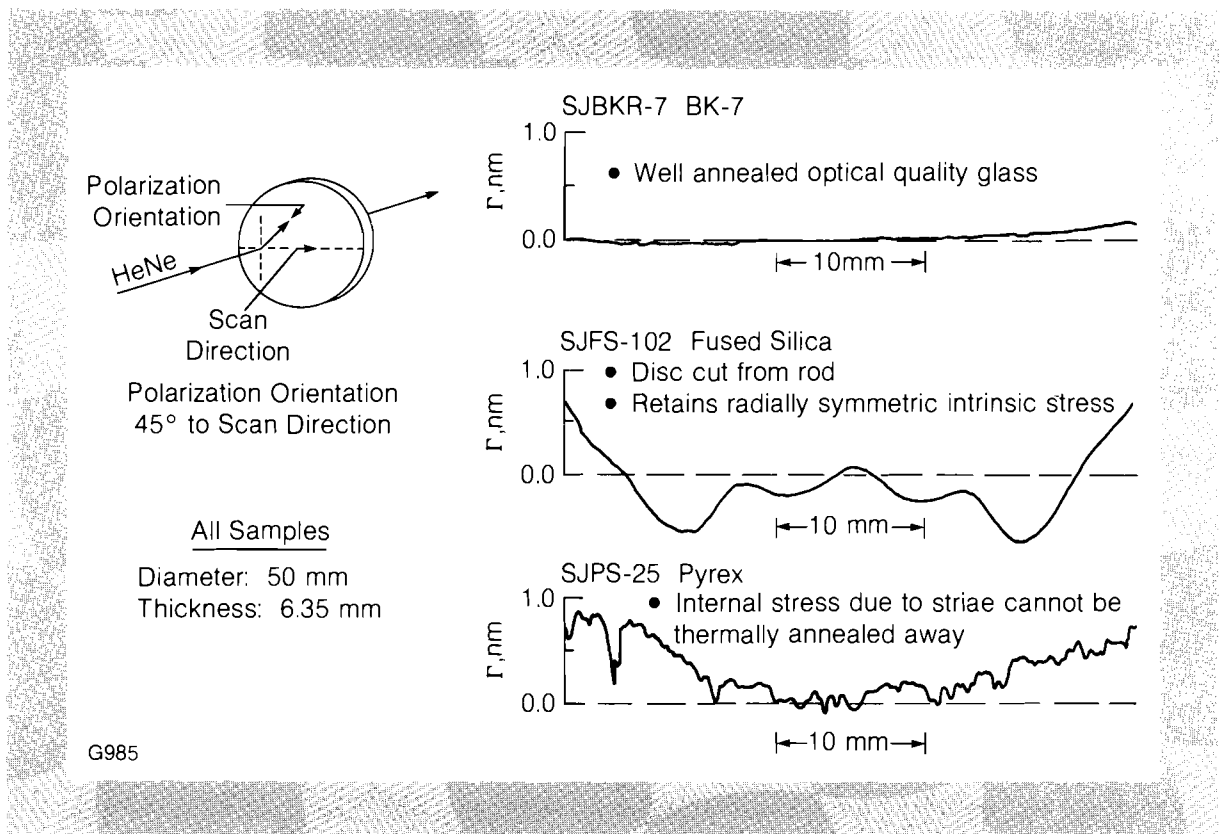
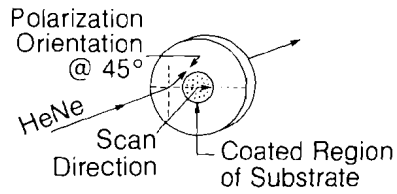


Fig. 3
Residual stress in standard thin film coating substrate materials. BK-7 and fused silica exhibit smoothly varying stress. The stress in "Pyrex" glass shows significant fine structure, making it less desirable as a coating substrate for modulated transmission ellipsometry.

Figure 4 gives the history of the evolution of stress in a coating substrate combination. Figure 4a shows the stress signature of a BK-7 substrate prior to coating. After e-gun evaporation of a $\text{Ta}_2\text{O}_5 - \text{SiO}_2$ multilayer thin film onto the substrate in vacuum at an elevated temperature of 200 °C, the sample exhibits the stress profile indicated in Fig. 4b. Only the central 12 mm diameter portion of the substrate has been coated, in order to show the change in stress across the diameter of the part in transition from uncoated to coated regions. Figure 4c shows the stress



- Substrate: 50 mm diameter × 6.35 mm thick BK-7
- Coating: HR_{45°} @ 351 nm and 1054 nm
- Materials: Ta₂O₅ and SiO₂
- Design: BK-7J (3H3L)⁴ 3H(LH)⁶ 2L
- Plotted data has been smoothed

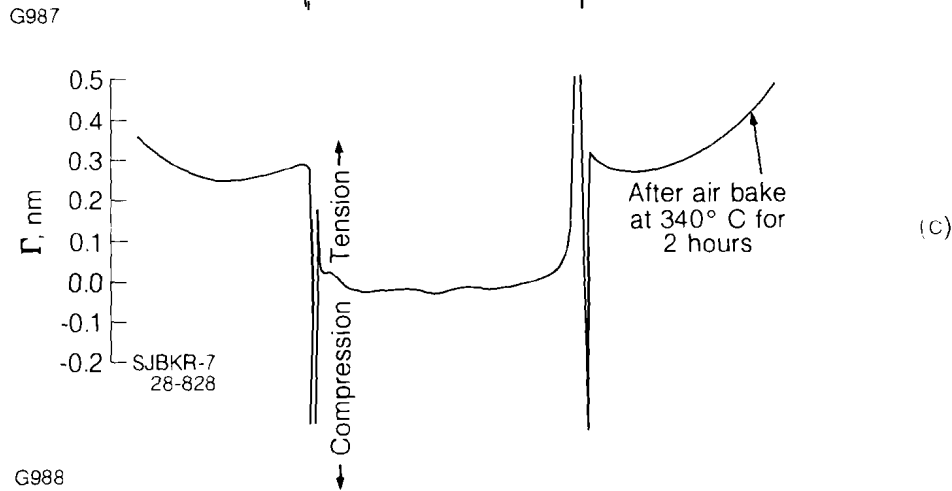
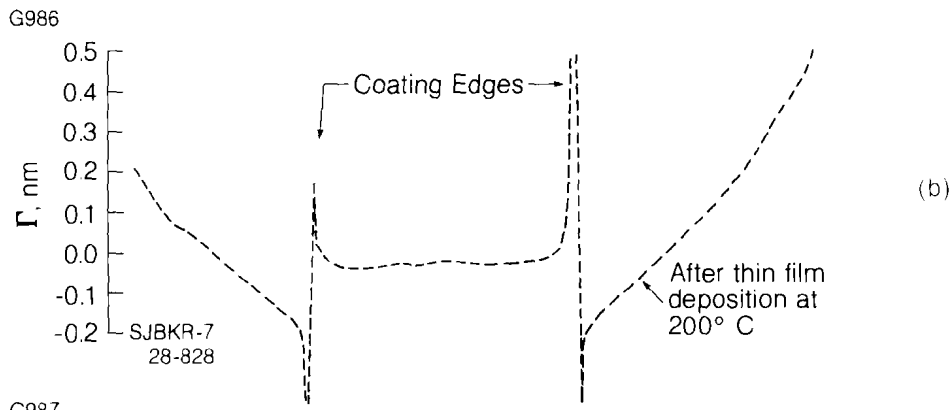
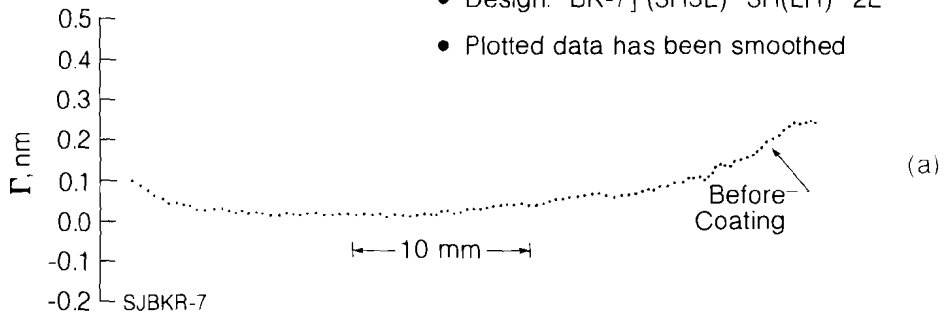


Fig. 4

Evolution of stress in a coating-substrate combination. The sign of stress within the coated region (tensile or compressive) can be inferred from the stress signature of the adjacent uncoated substrate.

- a) Optical retardance across substrate prior to coating.
- b) Stress induced in substrate after coating deposition at 200°C and exposure to room temperature and humidity.
- c) Sign reversal of stress in substrate caused by densification of coating during bake-out at 340°C.

Calibration of optical retardance in terms of tensile or compressive stress was done by measuring the sign of tensile stress in a TiO_2 ditch coating, after Lichtenstein³ and Heitmann.⁴

profile in this sample after an air bake at 340°C for two hours. Baking of oxide thin films is a standard processing procedure followed at many coating facilities. It helps to complete the oxidation of the evaporants, returning them to their proper stoichiometry. Baking also compacts and densifies the coating layers, driving out water vapor that is chemisorbed upon exposure of freshly coated samples to room temperature and humidity. A comparison of Figs. 4b and 4c shows that there is a reversal of sign to the stress in the BK-7 substrate adjacent to the coated region upon baking. We attribute this sign reversal to the densification process within the coating, in analogy with similar reversals observed by Heitmann for pure SiO_2 films.⁴

A preliminary explanation for the observed profiles is as follows: after deposition and exposure to ambient conditions the coating is in tension. Because it is too thick to deform and relieve the stress created at the coated surface, the uncoated substrate surface goes into compression in regions immediately adjacent to the coating. The sign of stress in the coating changes from tension to compression upon densification during air bake, and therefore the stress in the uncoated substrate adjacent to the coating changes sign to compensate.

There is one observation that does not fit in with the above explanation, and that is the lack of observable stress within the coated region itself. Perhaps the stress present at the coating surface is compensated for in the underlying substrate, and our measurement technique detects the net stress (being equal to zero) for the coating-substrate system. This compensation through the depth of the sample would not occur in uncoated areas where we see indirectly the stress in the coating from its effect on the uncoated adjacent surface.

Modulated transmission ellipsometry measures that component of stress within a sample which lies in a plane perpendicular to the probe beam propagation direction. In this work samples are oriented nearly normal to the probe beam, and the measurement is therefore sensitive to stress in the plane of the thin film coating. Figure 5 shows a retardance scan across a fused silica substrate which possesses a crazed or cracked coating. The stresses generated in the coating during air baking were either larger than the adhesion strength of the coating to the substrate, or exceeded the strength of the coating material itself. Crazing has relieved stress in localized regions of the coating surface, and we can determine the directionality of that stress which remains by varying the polarization of the probe laser. Figure 6 gives high-sensitivity, high-resolution scans across a central area of the coating from Fig. 5, taken with the HeNe probe laser polarized at 45° to the scanning direction (the same as that used in Fig. 5), and with the polarization parallel to the scanning direction. Both scans were generated along the same path across the coating. A photograph of the examined area is reproduced to the same horizontal scale immediately above the retardance scans.

Vertical craze lines 1 and 4 are *not* observed in the lower scan of Fig. 6, because the polarization orientation of the probe beam is parallel to the direction of stress relief immediately adjacent to these features. Op-

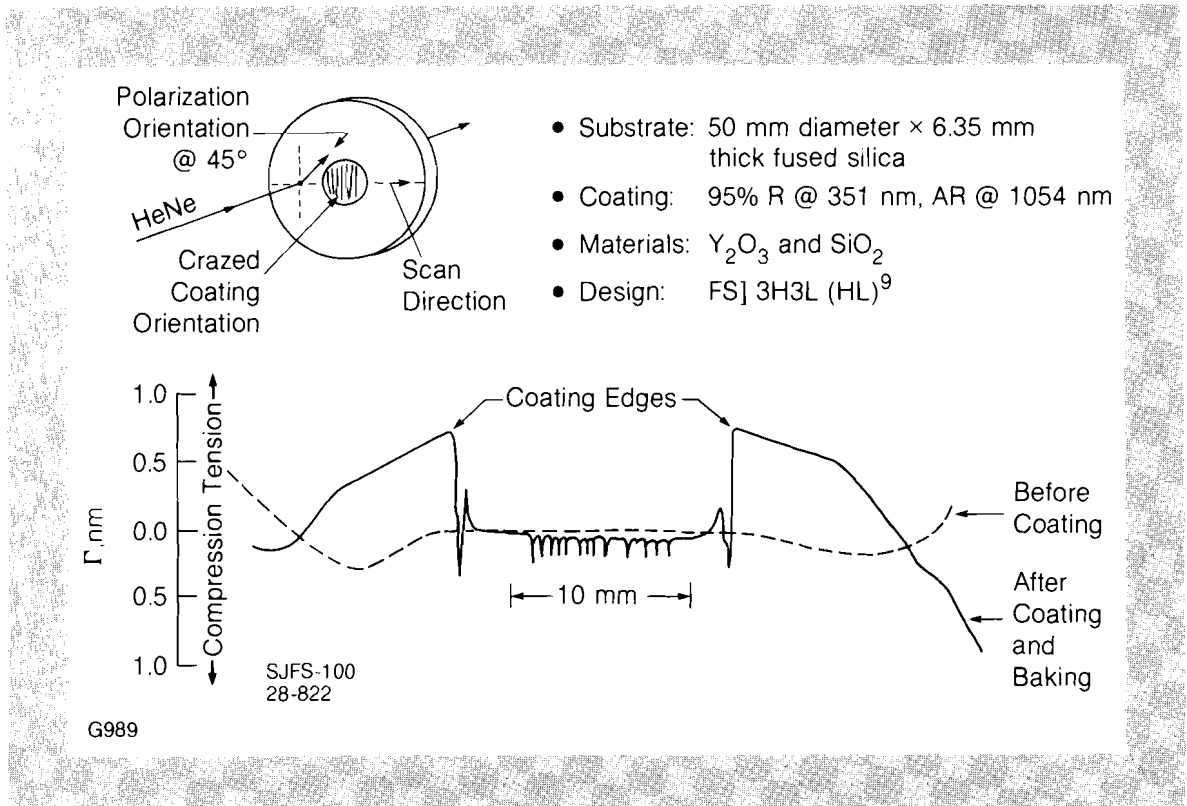


Fig. 5
Anisotropic stress in a crazed coating. A scan across the predominantly vertical craze marks with the probe beam polarized at 45° to the scan direction reveals that stress relief has occurred predominantly in a horizontal direction.

tical retardation can only occur if the probe laser polarization orientation is at some angle other than 0° or 90° to the coating stress. For this reason, the stresses associated with craze lines 2 and 3 are not easily observed with retardance measurements when the probe laser is polarized at 45° to the scanning direction.

Anisotropic stresses associated with absorbing defects in coatings can be mapped out using our modulated transmission ellipsometric technique, provided that the phase-sensitive signal is ratioed to the dc intensity emerging from the sample through the use of a pickoff plate as shown in Fig. 2. In the ratio mode of operation, the apparatus yields retardance data correct to within 10% of the actual coating retardance for defects which attenuate probe beam dc transmittance up to 40%. Figure 7 gives a two-dimensional representation of the compressive and tensile stresses associated with TiO_2 spatter sites embedded in a multilayer TiO_2 – SiO_2 high reflectance coating. The data has been plotted in $6\ \mu\text{m}$ by $6\ \mu\text{m}$ grids using a color code and shading scheme given in the legend adjacent to the plot. The stress patterns resemble the Nomarski microphotograph displayed above the 2-D plot, however, the stress does appear to extend over a larger area than that revealed by the photograph. There is a sudden change in film stress from tension to compression at the two defects in the figure and in the region between them. This feature is not detectable through standard optical microscopy.

No laser-induced damage tests have been conducted on absorbing defects for which an anisotropic stress map exists. It has been suggested¹ that, in such a test, regions initially in tension would exhibit a

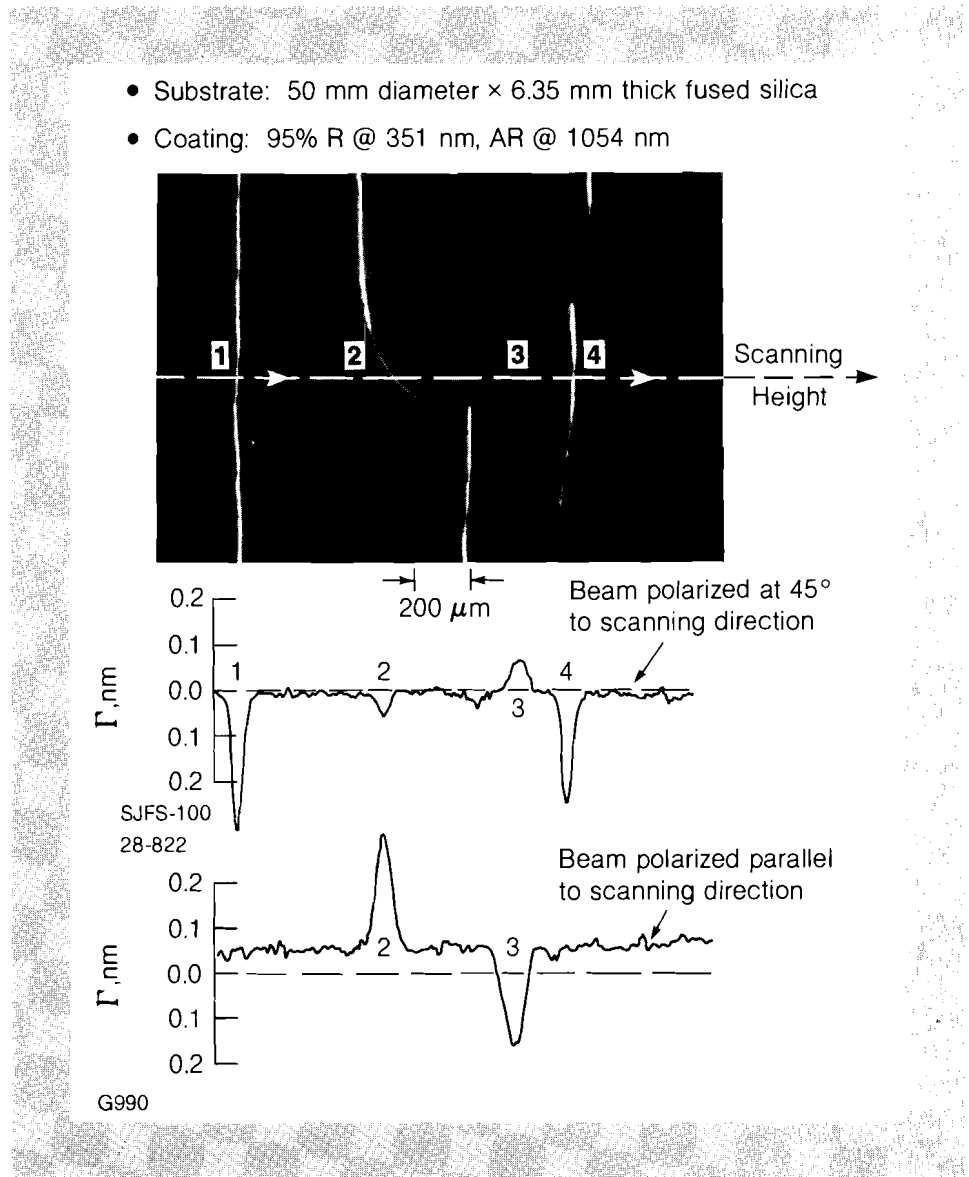


Fig. 6

Polarization sensitivity to stress in a crazed coating. High sensitivity scans across a central region of the coating from Fig. 5 show that the anisotropic stress associated with each craze mark is detectable when the probe beam polarization orientation is at some angle other than 0° or 90° to the cracks.

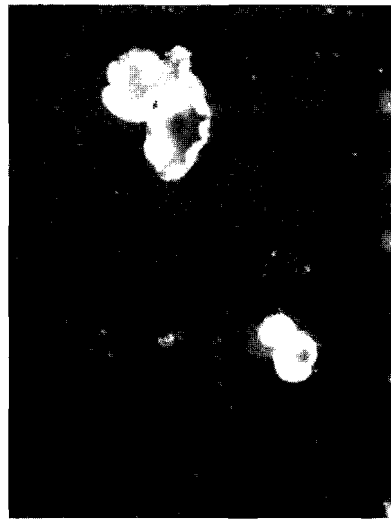
- a) Beam polarized at 45° to scanning direction—stress observable for craze marks 1 and 4.
- b) Beam polarized parallel to scanning direction—stress observable for craze marks 2 and 3.

The microphotograph is reproduced to the same horizontal scale as the retardance scans.

higher degree of damage resistance than those initially in compression, due to heat deposited in the absorbing defect and the resultant thermal expansion of the defect and adjacent coating material. In future work we intend to improve the resolution of our modulated transmission ellipsometer apparatus, map anisotropic stress associated with micron size absorbing defects, and correlate the magnitude and sign of anisotropic stress with laser-induced damage. An understanding of the relationship between anisotropic stress around defects and laser damage may enable us to improve the quality of our thin film coatings.

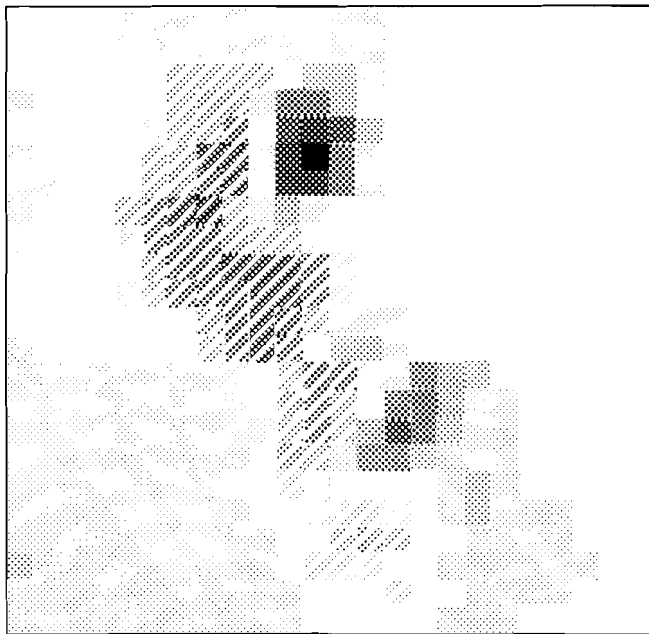
REFERENCES

1. A. Bloom and V. Costich, *NBS Publication 435: Laser-Induced Damage to Optical Materials*, 248 (1975).
2. R. Austin, R. Michaud, A. Guenther, and J. Putman, *Appl. Opt.* **12**, 665 (1973).



→ | 25 μm | ←

- Coating: $\text{TiO}_2/\text{SiO}_2$ multilayer
1.05 μm HR design
- Substrate: 50 mm diameter ×
1.6 mm thick plate
glass
- Polarization orientation @ +45°
to scan direction
- Data acquisition in ratio mode



Legend:

Γ, nm	COMPRESSION	TENSION
0.50-0.55		
0.40-0.49		
0.30-0.39		
0.25-0.29		
0.20-0.24		
0.15-0.19		
0.10-0.14		
0.05-0.09		
0.00-0.05		

G991

Fig. 7
Anisotropic stress around absorbing defects. The tensile and compressive nature of stress around two TiO_2 spatter sites in a multilayer dielectric thin film can be compared to a Nomarski microphotograph of the same region.

3. T. Lichtenstein, MS Thesis, Institute of Optics, University of Rochester, 1980.

4. W. Heitmann, *Appl. Opt.* **10**, 2685 (1971).

Section 2

PROGRESS IN LASER FUSION

2.A Irradiation Uniformity Experiments on OMEGA

Initial experiments on the 24-beam OMEGA laser system were conducted in 1981 with high intensities ($> 10^{15}$ W/cm²) on target, resulting in exploding pusher target implosions driven by long mean-free-path hot electrons. The increase in pulse length from 100 psec to 1 nsec in 1982 and the use of larger targets produced lower intensities (4×10^{14} W/cm²) which enable targets to be driven ablatively, i.e. a small fraction of the pellet mass is ablated outwards, driving the rest inwards like a rocket.

It is currently thought that spherical convergence of ablatively driven targets requires drive pressure uniformities (dP/P) on the order of a few percent. This in turn demands an irradiation uniformity (dI/I) of the same order, across the target surface. The OMEGA system permits this issue of uniformity to be addressed, since the on-target intensity distribution can be carefully diagnosed and controlled.

Perhaps the most surprising result of this series of experiments was that high aspect ratio targets (ratio of initial target radius to wall thickness = 200) could be compressed several hundredfold without breaking up. This is due to the high degree of irradiation uniformity provided by OMEGA.

Intensity Distribution on Target

It is difficult to directly measure the distribution of intensity across the target surface under full power conditions. Instead, a sample of each laser beam is photographed as it is focused onto a plane equivalent to

the target surface. A single representative distribution is chosen from the set of 24 such photographs, and is digitized and azimuthally averaged to yield a single radial beam profile. This profile is then analytically added over the surface of the target to give the intensity at any point on the target (see LLE Review, Volume 4).

The intensity distribution may also be expressed as a series of spherical harmonic functions. The coefficients of this expansion contain information about the spatial frequency of intensity nonuniformities. Modes with low spatial frequency will affect the gross shape of the core and are difficult to smooth, whereas high frequency modes may be smoothed but may drive hydrodynamic instabilities.

Such modelling of the intensity distribution permits the effects of laser parameters such as beam profile and focusing conditions to be determined, and to quantify the degree of nonuniformity.

Uniformity Experiments

A number of target shots were taken under carefully controlled conditions to assess the effects of irradiation uniformity on target performance. The targets were a homogeneous group of 400 μm diameter glass microballoons with 1 μm walls filled with 20 atmospheres of DT gas. The laser produced over 2 kJ on target in a 1 nsec pulse, and the standard deviation of the 24-beam energies was below 9%. Principal diagnostics were x-ray imaging through a pair of x-ray microscopes, and neutron yield measurements.

The program was divided into three main sets of experiments. The first two considered the effect of varying focus conditions and number of beams. The third set involved imposing intentional nonuniformities on the target.

Effects of Beam Focus

The point at which the beams are focused is described in terms of distance behind the center of the target, in multiples of the target radius, R . At approximately $3R$ focus, the beams begin to overlap their neighbors. At $8R$, each beam illuminates an entire hemisphere.

A series of shots was taken with the focus varied from $5R$ to $10R$. Figure 8 shows the time-averaged x-ray emission from the targets. At any instant of time, most of the emission will come from near the ablation surface. As the target implodes, this annular emission will progress inwards to the radius at which the ablation surface stagnates. At about this time, an expanding shock wave in the DT fuel strikes the inside of the shell, causing an emission there. In between these two points, corresponding to the cold compressed shell, there should be no emission. Indeed, in the lower photograph in Fig. 8, such a nonemitting ring is evident, indicating that the shell remains intact during the implosion. However the upper photograph, corresponding to $6R$ focus, shows no such feature, indicating that the shell is probably breaking up.

Figure 9 shows the amplitudes of the spherical harmonic components of the illumination nonuniformity for the two cases shown in Fig. 8.

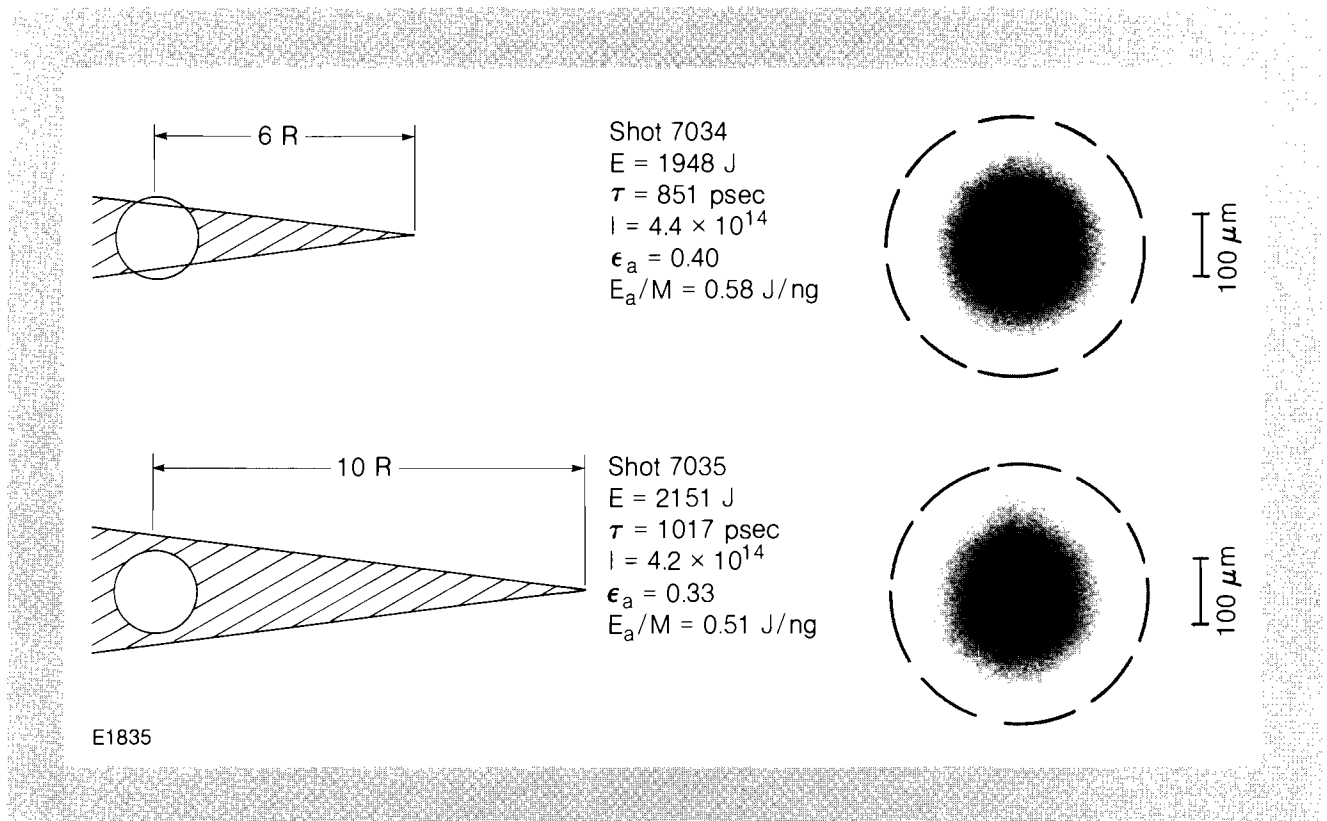


Fig. 8
 Photographs of the x-ray self-emission of $400 \mu\text{m}$ diameter targets taken with x-ray microscopes show the integrity of the shell when the irradiation is sufficiently uniform. The two micrographs show targets irradiated under different focus conditions. Only the 10R shot shows a well-defined stagnated shell. The symbols used in this and subsequent figures are: E (energy on target), τ (laser FWHM pulse width), I (average intensity on target), ϵ_a (fraction of incident energy absorbed by the target), E_a/M (specific absorbed energy, i.e. absorbed energy divided by target mass).

The dominant mode at $\ell=8$ is a consequence of the 24-beam OMEGA geometry. All modes have greater amplitudes for the 6R focus than for 10R, suggesting that 10R should provide more uniform illumination. This is borne out by the results in Fig. 8.

Number of Beams

The second set of experiments was designed to determine how the number of beams on target affected target performance. Targets were irradiated at 10^{14} W/cm^2 with 6, 12, and 24 beams. As the number of beams was increased, individual beam energy was reduced to maintain the same power on target.

Figure 10 shows the x-ray emission from targets irradiated with 6, 12, and 24 beams. The 6-beam shot shows the imprint of the beams outside the core, and the nonemitting ring around the core is poorly defined. On the other hand, the core is better defined in the 24-beam case, indicative of better uniformity. The 12-beam shot is intermediate.

Figure 11 shows the ℓ -mode amplitudes corresponding to these three shots. Clearly the 24-beam case is best. The biggest contribution to non-uniformity for the 6-beam set is the $\ell=2$ and $\ell=4$ modes, which should produce visible structure on the target, as is seen.

It should be noted that these results, indicating that ≥ 12 beams are required for uniform compression, are dependent on the OMEGA beam geometry and $f/3$ lenses. The 24-beam geometry, in which neighboring beams are not equidistant, is different from a regular polyhedron with,

Fig. 9
 The standard deviation of the intensity distribution is decomposed into spherical harmonic components for the two shots shown in Fig. 8. Higher ℓ -modes correspond to nonuniformities with higher spatial frequencies.

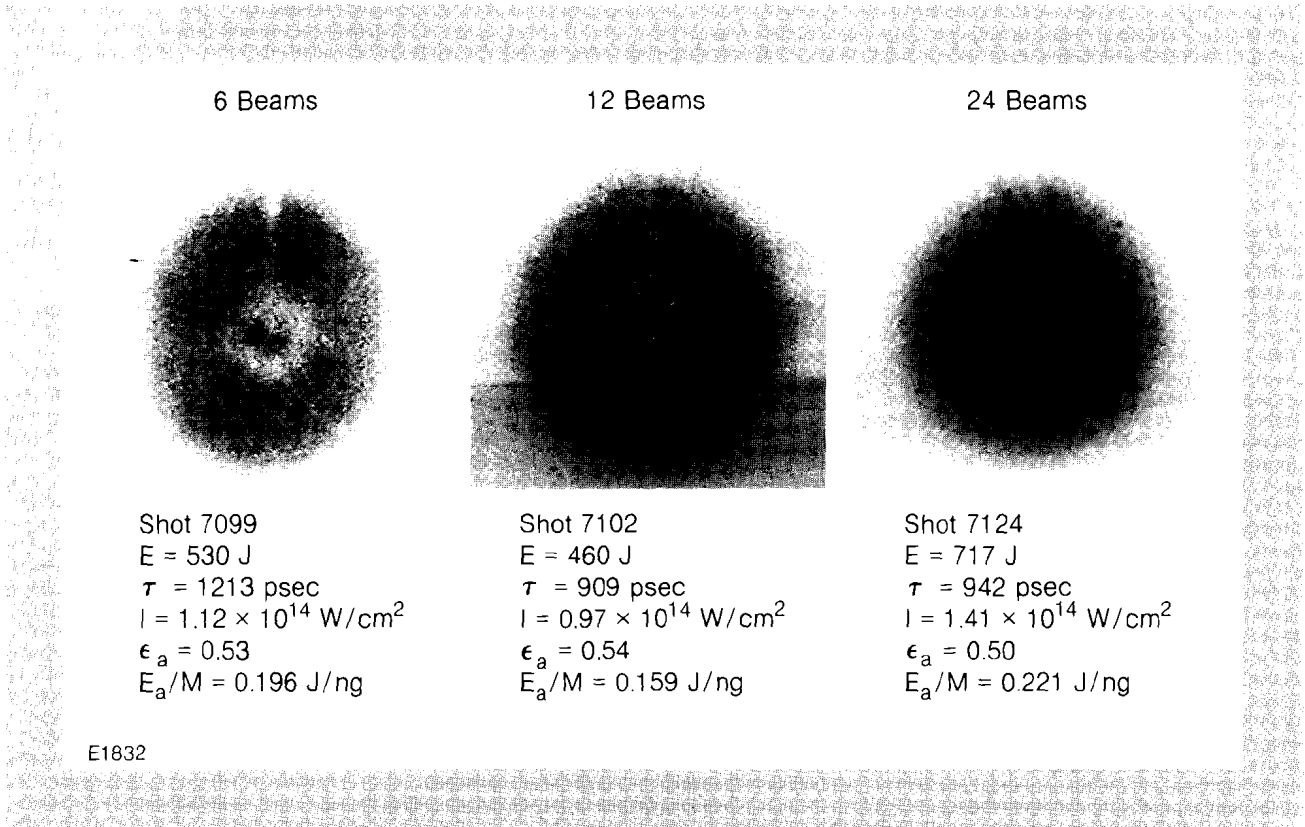
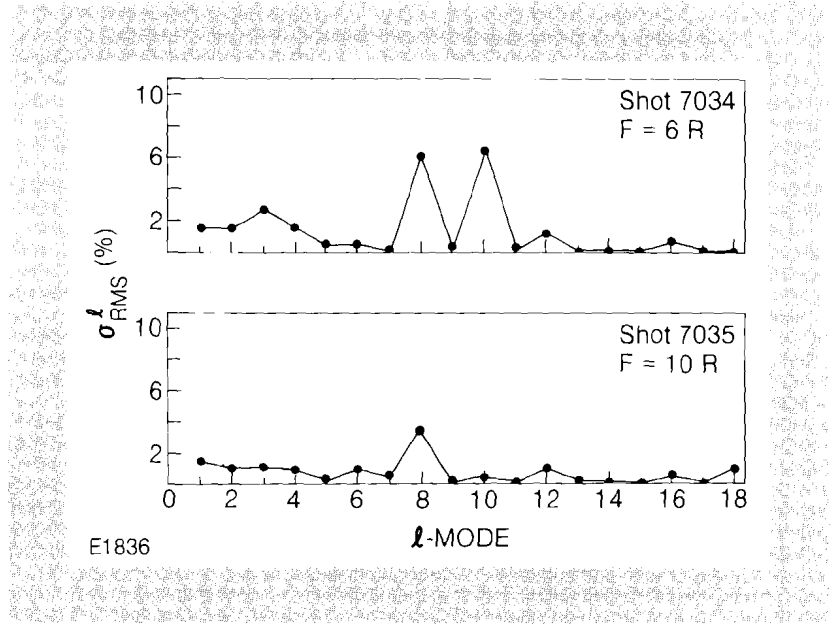


Fig. 10
 X-ray micrographs of targets irradiated with the same average intensity but differing numbers of beams show improved target performance with larger numbers of beams.

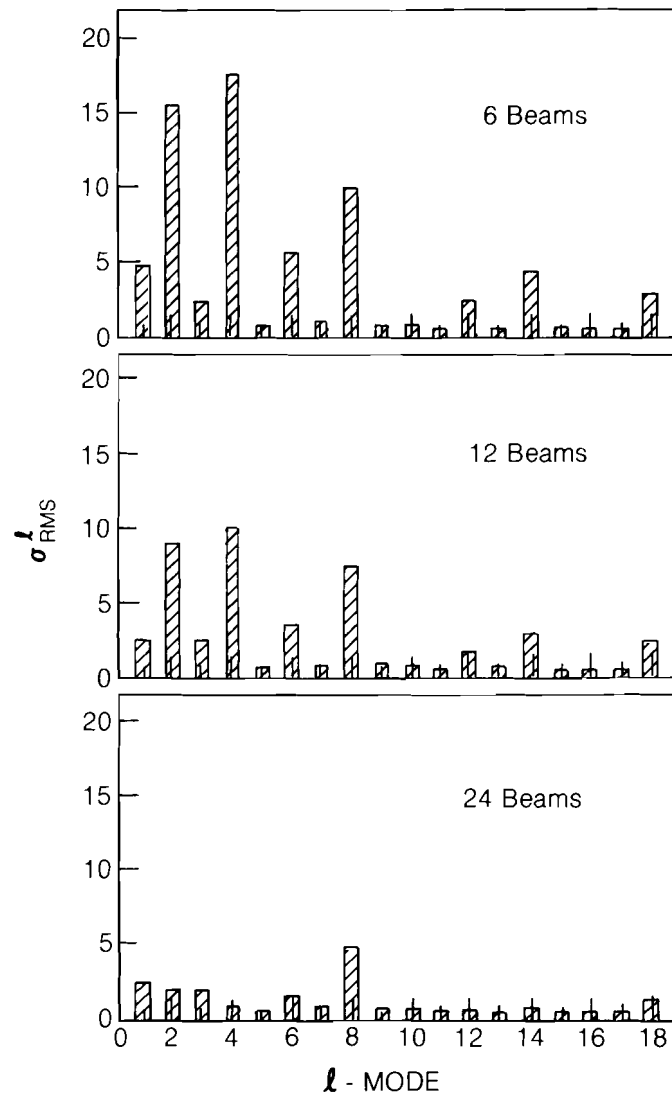


Fig. 11
Spherical harmonic contributions to the intensity uniformity confirm that irradiation uniformity is improved with larger numbers of beams.

say, 20 faces. There may be conditions in which such a regular geometry may produce even better irradiation uniformity. However, the 24-beam geometry was chosen because it is less sensitive to focus conditions than the 20-beam set.

Figure 12 shows the neutron yield for shots with intensities near 10^{14} W/cm², versus number of beams. There is a significant increase from N = 6 to N = 12, and a small one from N = 12 to N = 24. However, neutron yield is a rather poor indicator of irradiation uniformity, since with these targets, most of the yield is produced by a shock wave before peak compression of the fuel, and the shock shape is relatively insensitive to drive nonuniformity.

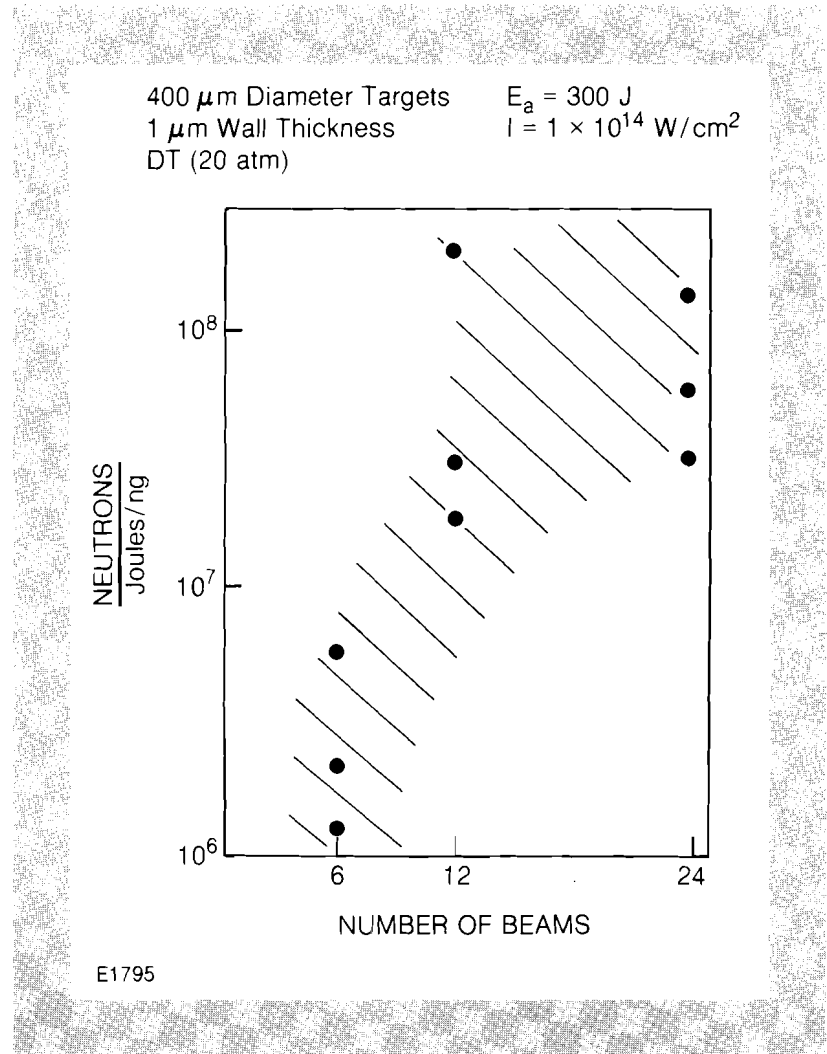


Fig. 12
 Neutron yield, normalized to specific absorbed energy, is plotted versus number of beams for shots taken with intensities near 10^{14} W/cm^2 .

Intentional Nonuniformities

It is possible to excite low order nonuniformities by adjusting individual beam energies. Such modes should produce visible deformities in the core. $\ell = 1$ modes are driven by imbalancing opposing beams. For the shot shown in the right-hand x-ray micrograph in Fig. 13, the intensity on the left-hand side of the target was reduced by a factor of two. Because the absorption is somewhat higher with lower intensity, the actual drive difference is less than a factor of two, giving an $\ell = 1$ amplitude of 22%. Compared with the balanced shot also shown in Fig. 13, it can be seen that the core is shifted to the left, and the cool region descending from the mounting stalk describes a curved trajectory.

The brightest x-ray emission comes from the inside of the stagnated shell on the low-intensity side. This is most likely due to a shock launched from the high-intensity side colliding with the opposing wall. In spite of the severe asymmetry, neutron yield was only reduced by a factor of two for this shot.

$\ell = 2$ modes were driven by irradiating targets with two opposing clusters of 4 beams each, as shown in Fig. 14. The two views indicate that

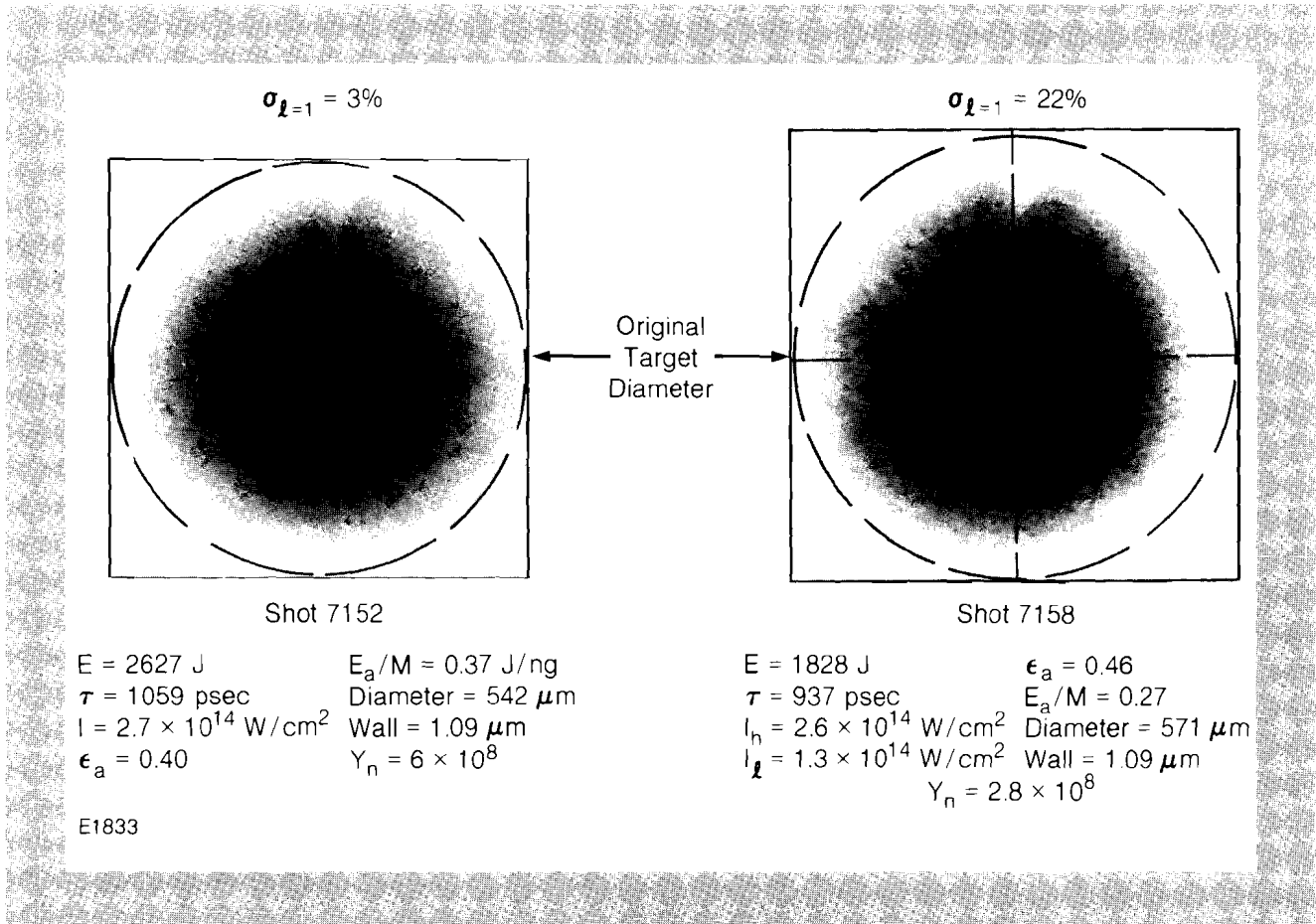


Fig. 13

The intensity on the left side of the target (I_l) was intentionally reduced from that on the right (I_n) in order to observe the effects of an $l=1$ mode. The left-hand target is under normal irradiation conditions, while the right-hand target has a 22% $l=1$ mode. The core is clearly decentered due to this imbalance.

the core is pancake-shaped. Clearly this 8-beam set is much worse than the symmetric 6-beam set shown in Fig. 10. Again, the neutron yield was not seriously degraded, showing that even a severely perturbed core does not affect the shock-produced yield.

Summary

The symmetric compression of high-aspect ratio shells has been demonstrated on OMEGA. The shell integrity is affected by focus conditions, and at least 12 beams are required to produce symmetric implosions. Intentional illumination asymmetries were used to study their effects on gross core shape.

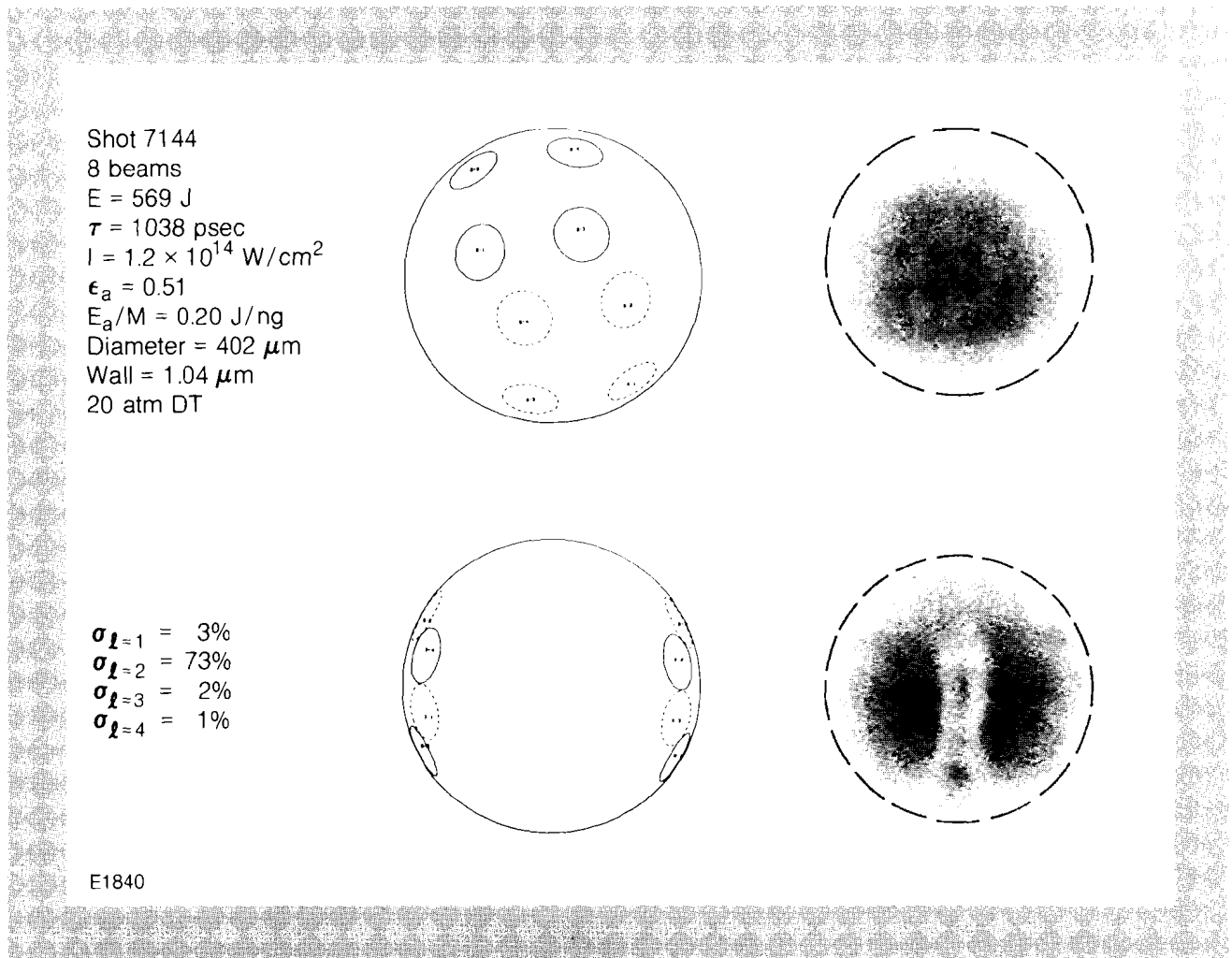


Fig. 14
 Two views of the same target irradiated with 8 beams show that the core is pancake-shaped, due to the 73% $\ell=2$ mode.

2.B Thermal Smoothing of Irradiation Nonuniformities in Laser-Driven Fusion

Spherical targets must be irradiated with a high degree of uniformity to drive the high-density implosions required for commercial energy production by laser fusion. Although completely spherical illumination can never be attained, some nonuniformities in laser energy-deposition on target can be smoothed by thermal conduction^{1, 2} as the heat is transported from the surface of laser deposition (at the critical density) to the ablation surface where the implosion is driven. The amount of thermal smoothing is influenced by inhibition of the thermal heat-flow into the target. Computer simulation of experiments and transport-theory have shown that the heat-flux is reduced relative to the classical Spitzer-Härm result, and that it saturates (or is "flux-limited") at a value far below the limit for freely streaming electrons.³ The inhibition will have two competing effects on thermal smoothing: (1) the distance available

for smoothing is reduced due to a smaller separation between the critical and ablation surfaces,⁴ but (2) with less heat flowing radially into the target, more is available to flow laterally and to smooth nonuniformities. Using a model of steady-state ablation and thermal transport,⁴ the second process is found to dominate. It reduces the laser intensity required for adequate thermal smoothing, substantially below the value estimated using classical transport. For even short-wavelength irradiation, this should permit laser operation below the intensity at which energetic electrons from resonance absorption would preheat the target and preclude a high-density compression.

The smoothing of a temperature nonuniformity is calculated here, first without the complication of hydrodynamic motion to demonstrate the effect of flux-limited transport; and this is followed by a more realistic treatment of the laser ablation process. For the simple model, steady-state heat-flow is assumed in the z-direction through a plasma of constant density with a temperature profile $T_0(z)$. A perturbing heat-source S' is imposed at $z = 0$, where $S' = S_0 \cos(ky) \delta(z)$ and k is the perturbation wave number in the transverse (y) direction. For classical transport, the heat-flux is given by the Spitzer-Härm result,⁷

$$\bar{q} = -\kappa T^{5/2} \nabla T \tag{3}$$

where T is the electron temperature and κ is the coefficient of thermal conductivity. The heat flux saturates at a value of q_{\max} , usually parameterized in the form:

$$\bar{q}_{\max} = -f n_e v_{th} T |\nabla T| \tag{4}$$

where the factor f (flux-limiter) is an adjustable parameter; n_e is the electron number density, and v_{th} is the electron thermal velocity ($\sqrt{T/m_e}$). Typically, values of f between 0.03 and 0.06 have been used to interpret experiments³—an order of magnitude below the value 0.65 for an isotropic, free-streaming gas. Using Eqs. (3) and (4), and $\nabla \cdot \bar{q} = S'$, the following equations are obtained for classical and flux-limited transport to first order in the perturbed temperature T' (where $T = T_0 + T'$):

$$\frac{d^2}{dz^2} (T_0^{5/2} T') - k^2 (T_0^{5/2} T') = 0 \tag{5a}$$

$$\frac{d}{dz} (\sqrt{T_0} T') + \frac{2}{3} k^2 L (\sqrt{T_0} T') = 0. \tag{5b}$$

Here $z > 0$, $\nabla T_0 / |\nabla T_0| = -1$, T' has $\cos(ky)$ y-dependence, and L is the unperturbed temperature scale-length, i.e., $L = T_0 |dT_0/dz|^{-1}$. Solving Eqs. (5a) and (5b) for constant L , a comparison can be made between the different attenuations, $A = T'(z)/T'(0)$, of the temperature nonuniformity:

$$A \sim e^{-kz} \tag{classical} \tag{6a}$$

$$A \sim e^{-Lk^{2/3}z} \tag{flux-limited} \tag{6b}$$

The important difference between classical and flux-limited thermal smoothing is the linear versus quadratic dependence on wave number. Both attenuations show increased smoothing for short-wavelength perturbations due to the proximity of hot and cold regions, but the distance required for smoothing decreases with k more rapidly for saturated flow, by a factor $\sim kL$. From the steady-state ablation model below, kL corresponds to ~ 4 for the nonuniformity characteristic of multiple, overlapping laser beams. For that example, flux-limited transport enhances the lateral heat-flow, and the required separation distance for smoothing is several times shorter than the classical result.

The thermal smoothing calculation for a realistic laser fusion model must include the effects of hydrodynamic motion and spherical geometry. To approximately treat the ablation process, an analytic, steady-state model by Max et al.⁴ was used to obtain the spherically symmetric, unperturbed density (ρ_o) and temperature (T_o) profiles. The energy equation used for transport between the critical and ablation surfaces is:

$$\frac{5}{2} \rho \bar{v} \cdot \nabla T / \mu + \nabla \cdot \bar{q} = 0 \quad (7)$$

where μ is the average mass per particle; and terms on the order of $\mu v^2/T$ have been neglected as fluid flow inside critical density is highly subsonic for small flux limits. This model divides the region between the critical and ablation surfaces (at radii R_c and R_a) into two parts at the point R_s where the classical and flux-limited heat flows are equal. Between R_c and R_s the heat-flux is saturated while it is classical between R_s and R_a . In the flux-limited region:

$$T_o(r) = T_c (r/R_c)^{4/(1+M^2)} \quad (8)$$

where T_c is the temperature at critical density; and M is the Mach number (given approximately by $M \cong 14f$ for a CH_2 plasma).

Nonuniform laser deposition at the critical surface produces a perturbed temperature T' . Expanding T' in spherical harmonics,

$$T'(r, \theta, \phi) = \sum T_{\ell m}(r) Y_{\ell m}(\theta, \phi) \quad (9)$$

the perturbed energy transport equation in the flux-limited region becomes:

$$\frac{d}{dr} T_r - 2 \frac{\ell(\ell+1)}{r^2} \frac{T_o}{dT_o/dr} T_r - 2 \frac{\dot{m}'}{\dot{m}} \frac{d}{dr} T_o = 0 \quad (10)$$

where \dot{m} is the mass ablation rate $4\pi r^2 \rho_o v_o$. Only the subscript ℓ has been kept, since the equation is independent of the azimuthal index. The quantity \dot{m}' is the perturbed mass ablation rate $4\pi r^2 (\rho v_r)'$, and it can be evaluated by solving the full set of perturbed hydrodynamic equations.¹⁰ However, for these calculations, the simplifying assumption was made that \dot{m}' varies with perturbed temperature according to:

$$\dot{m}' = \xi \dot{m} T' / T_o \quad (11)$$

with ξ being an adjustable parameter to determine the sensitivity of the results to \dot{m}' . This form gives the correct functional dependence of T' for $\ell=0$ when $\xi = 1/2$ in the flux-limited region, and when $\xi = 5/2$ in the classical region. Over this range of ξ , the results below are relatively insensitive to \dot{m}' for the dominant mode of irradiation nonuniformity.

Attenuation of temperature nonuniformities due to flux-limited transport is obtained by substituting Eqs. (11) and (8) into Eq. (10). For a small separation distance of the flux-limited region, ($\Delta R_s \equiv R_c - R_a$) the relative temperature attenuation at R_s is:

$$\left[\frac{T_\ell}{T_0} \right]_s = \left[\frac{T_\ell}{T_0} \right]_c \times \exp \left\{ - \left[\ell(\ell+1)(1+M^2)/2 + 8(\xi - 1/2)/(1+M^2) \right] \frac{\Delta R_s}{R_c} \right\}, \quad (12)$$

This expression displays the same quadratic dependence on wave number, $k \sim \ell$, as Eq. (6b). Temperature attenuation in the classical region was evaluated numerically and found to contribute less than 10%, for small flux-limiters ($f \leq 0.06$). Thus, Eq. (12) well approximates the total thermal smoothing.

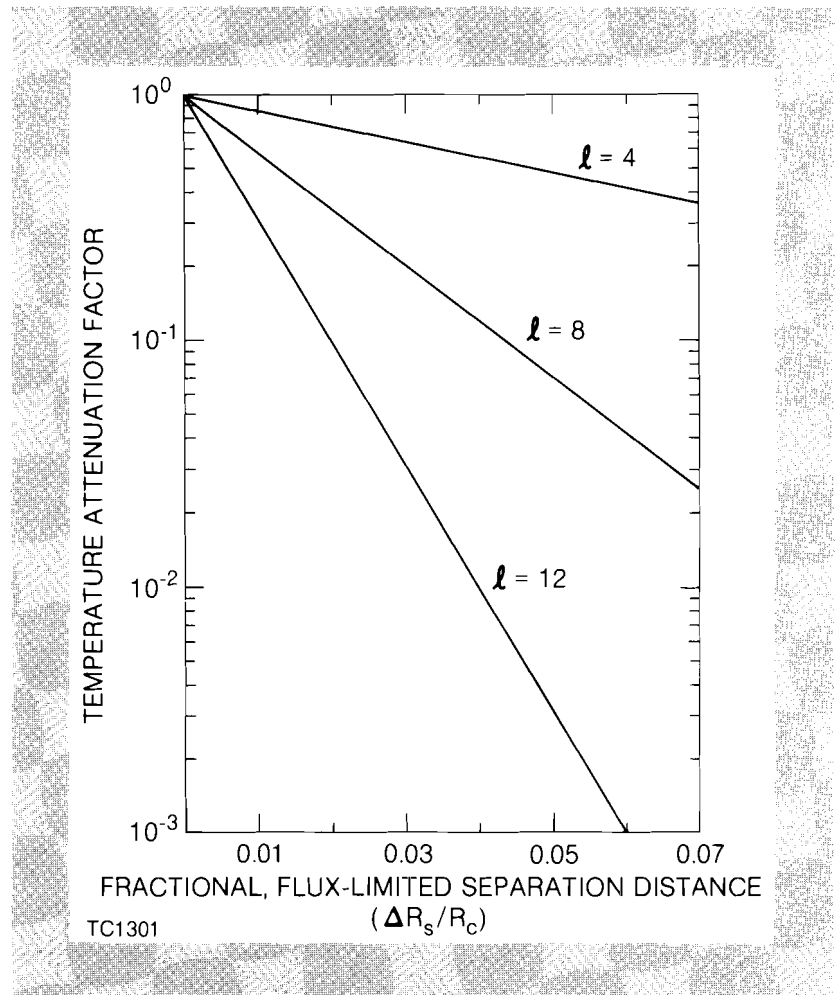


Fig. 15
Dependence of the nonuniform temperature attenuation on the radial separation distance of the flux-limited region for different spherical harmonic modes of the laser-deposition nonuniformity (Eq. 12). The parameter ξ was set to 1/2 so that the results are relative to zero attenuation for the $\ell=0$ mode.

The temperature attenuation in the flux-limited region (Eq. 12) is shown in Fig. 15 as a function of the fractional separation-distance, $\Delta R_s/R_c$, for the modes $\ell = 4, 8$ and 12 with $\xi = 1/2$. Typically, for illumination with ~ 20 overlapping, uniformly-distributed laser beams, $\ell \sim 8$ is the dominant mode of nonuniformity,^{8, 9} corresponding to a nonuniformity wavelength about equal to the target radius. (The dominant mode is related to the number of beams N approximately by $\ell \sim 2\sqrt{N}$.) For $\ell = 8$, a ten-fold attenuation is obtained when the separation distance of the flux-limited region is ~ 0.04 times the target radius. The relation between $\Delta R_s/R_c$ and the laser intensity is shown in Fig. 16 for different flux-limiters, at a laser wavelength λ of $0.35 \mu\text{m}$ and a target radius of $500 \mu\text{m}$. For other radii and laser wavelengths, the intensity varies roughly as $R_c/\lambda^{3.5}$.

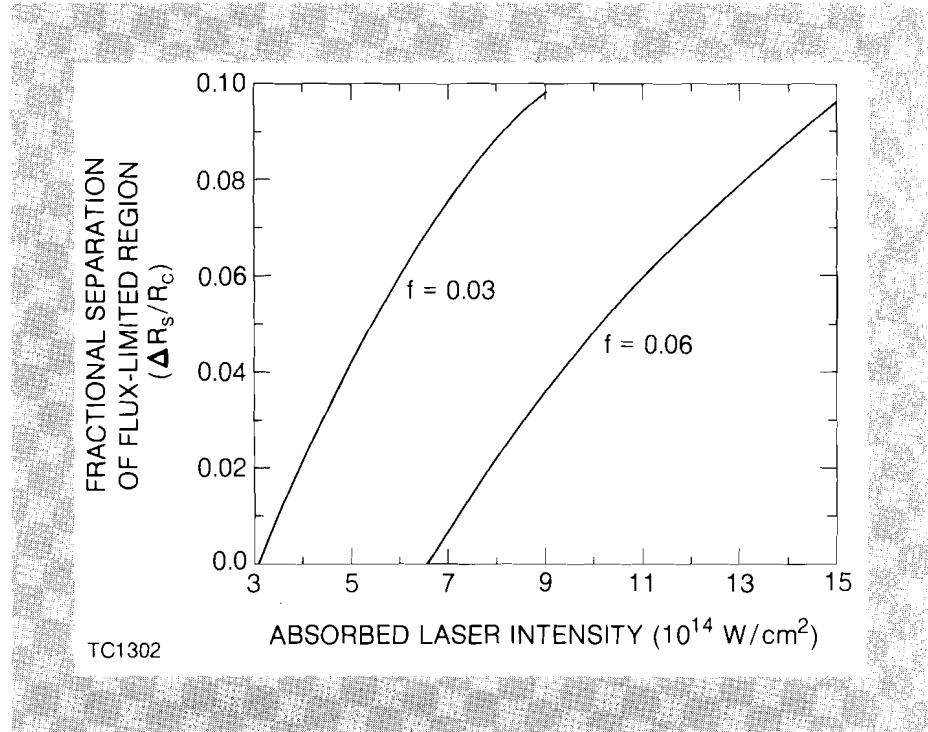


Fig. 16

Relation between the laser intensity and the radial separation distance of the flux-limited region for different flux-limiters. The results used the steady-state ablation model of Max et al.⁴ for the target radius $R = 500 \mu\text{m}$ and the laser wavelength, $\lambda = 0.35 \mu\text{m}$. For other values of R and λ , the laser intensity scales roughly as $I \sim R/\lambda^{3.5}$.

From Figs. (15) and (16), an order of magnitude smoothing is obtained at laser intensities around $5 \times 10^{14} \text{W/cm}^2$ for low flux-limits ($f \leq 0.06$). These irradiances are about ten times lower than the classical estimates.^{11, 12} Although a small flux-limit is known to degrade the implosion-efficiency, it is seen here to have at least one positive feature—it can enhance the smoothing of laser nonuniformities.

The sensitivity of this result to the approximate treatment of \dot{m}' (Eq. 11) is summarized in Table 2, which shows the intensity at which the $\ell = 8$ mode is attenuated ten-fold for $\xi = 0, 1/2$ and $5/2$. The variation in intensities with ξ is relatively small compared to the effect of the flux-limiter, and this justifies, in part, the simplified treatment of \dot{m}' . In contrast, for $\ell = 2$, the perturbed mass ablation rate strongly affects the amount of temperature attenuation, and any results for this mode are very model-dependent.

These results suggest that adequate smoothing of the dominant $\ell = 8$ nonuniformity from ~ 20 -beam illumination can occur at moderate laser

Table 2

The intensity (10^{14} W/cm²) at which an $\ell = 8$ nonuniformity in laser energy deposition is attenuated for different flux-limiters, f , and parameters ξ from the perturbed mass ablation rate (Eq. 11). (The critical radius is $500 \mu\text{m}$, and the laser wavelength is $0.35 \mu\text{m}$.)

$f \backslash \xi$	0	1/2	5/2
0.03	5.2	4.7	4.2
0.06	8.2	8.0	7.5

TC1403

intensities and short-wavelengths. An important question not addressed here is the effect of laser illumination before a sufficient smoothing distance is established. This transient effect requires time-dependent calculations (presently in progress) of the full implosion process. A calculation² for one target design has shown that illumination nonuniformities imprint themselves on the target surface early in time and degrade the thermonuclear burn due to a nonspherical compression. During the implosion, the time at which thermal smoothing becomes effective depends on the details of electron energy-transport, as demonstrated above. A more detailed calculation would include the effects of non-local electron transport. Although the models used here only approximate the laser fusion process, they identify some of the important mechanisms that contribute to thermal smoothing. The results show that thermal smoothing depends on much more than the distance between the critical and ablation surfaces. Smoothing is crucially dependent on the size and temperature scale-length of the flux-limited region.

The reduction obtained in intensity required for thermal smoothing is particularly important for laser fusion experiments using short-wavelength illumination (such as $\lambda = 0.35 \mu\text{m}$ from frequency-tripled Nd:glass lasers.) Present interest in using short-wavelength laser light is motivated by the high classical absorption and high hydrodynamic efficiency for imploding the target¹³; and the main drawback has been the prospect of poor thermal smoothing at moderate laser intensities.¹² Classical estimates placed the required intensity for smoothing near 10^{16} W/cm², at which point, high-energy electrons from resonance absorption are expected to preheat the target and degrade the implosion. By including the effects of flux-limited heat-flow, the required intensity for $0.35 \mu\text{m}$ illumination is reduced to about 5×10^{14} W/cm² where the generation of damaging suprathermal electrons should be negligible.

REFERENCES

1. D. B. Henderson and R. L. Morse, *Phys. Rev. Lett.* **18**, 355 (1974).
2. W. C. Mead and J. D. Lindl, "Symmetry and Illumination Uniformity Requirements for High-Density Laser-Driven Implosion", *LLNL Report UCRL-78459* (1976), unpublished.
3. D. Shvarts, J. Delettrez, R. L. McCrory, and C. P. Verdon, *Phys. Rev. Lett.* **47**, 247 (1981) and references therein.
4. C. E. Max, C. F. McKee, and W. C. Mead, *Phys. Fluids* **23**, 1620 (1980).

7. L. Spitzer and R. Härm, *Phys. Rev.* **89**, 977 (1953).
8. S. Skupsky and K. Lee, "Illumination Uniformity by Multiple Overlapping Beams for Laser-Driven Fusion", manuscript in preparation.
9. R. Kidder, *Nucl. Fusion* **16**, 1 (1976).
10. See techniques discussed in: R. L. McCrory, R. L. Morse, and K. A. Taggart, *Nucl. Sci. Eng.* **64**, 163 (1977) and D. B. Henderson, R. L. McCrory, and R. L. Morse, *Phys. Rev. Lett.* **33**, 205 (1974).
11. M. H. Emery, J. H. Orens, J. H. Gardner, and J. P. Boris, *Phys. Rev. Lett.* **48**, 253 (1982).
12. J. H. Gardner and S. E. Bodner, *Phys. Rev. Lett.* **47**, 1137 (1981).
13. R. L. McCrory and R. L. Morse, *Phys. Rev. Lett.* **38**, 544 (1977).

Section 3

DEVELOPMENTS IN MICROFABRICATION

3.A Biased Sputtering of Target Pusher Layers

Many laser fusion target designs call for metal pusher layers which have surface roughnesses of less than 50 nm and thickness uniformities of a few percent. Applying coatings which meet these requirements to spherical glass microballoons is a unique challenge. One reason for this is the problem which arises when the coating material is deposited on a surface at oblique angles of incidence, as it must for a spherical substrate. In this situation, small defects in the surface tend to shadow the surrounding area, and therefore grow preferentially with respect to the background.^{1, 2} The rapid growth of these defects can lead to unacceptably rough surfaces.

Another variable in the coating process is the mobility of the atoms which arrive at the surface. This mobility is a function of the substrate temperature, energy of the incident atoms, and the reactivity of the metal with impurities such as oxygen and nitrogen which always exist in a coating environment. If the mobility is too low, the coating grows in columns, aggravated by the oblique incidence problem discussed above. This produces an underdense layer with a rough surface. If the mobility is too high, macrocrystallites grow, which also leads to a rough surface.³

An approach which we have been exploring, in order to gain greater control over the growth of defects and surface mobility, is the use of a bias voltage applied to the microballoon during sputter coating. Biased sputtering, as this is called, is a common practice in many coating applications,^{4, 5, 6} but this is the first time, to our knowledge, that it has been

used in pusher layer fabrication. The principle is quite simple. A film being grown by sputtering is bombarded by ions and neutral atoms of both the depositing metal and the background sputter gas (usually Ar). By applying an accelerating (negative) voltage to the substrate, the ions can be made to arrive more nearly normal to the surface, and they will impart energy to the growing film, thereby increasing the adatom mobility. There is considerable evidence^{4, 5} that bias sputtering can dramatically alter the quality of deposited films. This led us to examine its effect in pusher layer fabrication.

The apparatus used for our experiments is illustrated in Fig. 17. The vacuum system consists of a cylindrical stainless steel chamber, 40 cm in diameter by 30 cm high, pumped by a cryo-baffled 15 cm diffusion pump. The sputtering source is a Sloan model S-310 magnetron, operated at a dc power of 340 watts. The system is pumped to a base pressure of 2×10^{-4} Pa or below prior to each run. The system is operated at a pressure of 1.0 Pa using purified Ar. The stalk-mounted microballoons are located 7.5 cm directly below the center of the S-310, and are rotated as shown in Fig. 17. A sliding contact allows the microballoon to be biased during coating. No pre-coating of the microballoon or stalk was done; therefore biasing does not occur until a continuous conducting film, tens of nm thick, has been deposited on both the stalk and microballoon.

Fig. 17
Illustration of the apparatus used to sputter coat-biased microballoons. The stalk-mounted microballoon is located 7.5 cm below the magnetron sputter source and is rotated about a horizontal axis as shown. Negative biases of up to 100 V can be applied to the microballoon during coating.

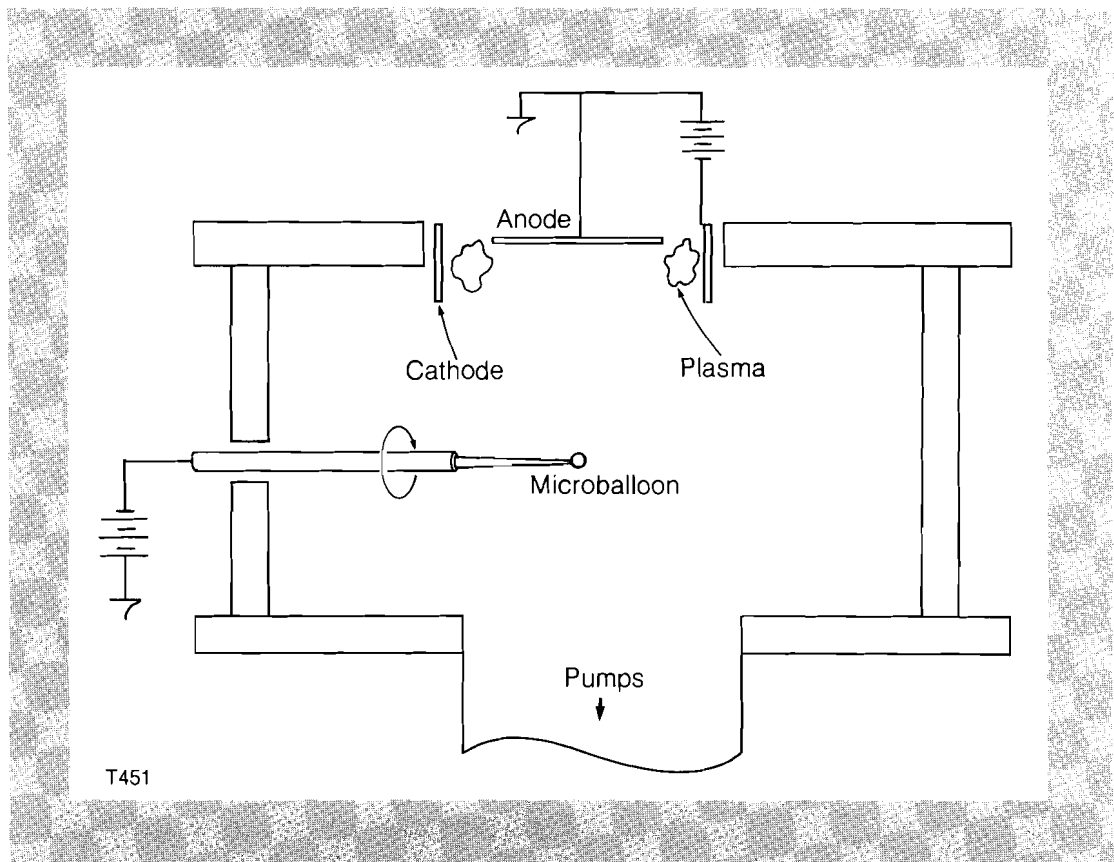


Figure 18 shows scanning electron micrographs of Ni coatings applied under otherwise identical conditions, without bias (a) and biased at -100 V (b). Figure 18a illustrates the columnar growth and resulting

rough surface which is evidence of limited surface mobility. In Fig. 18b, the biased case, we see a much denser microstructure and smoother surface.

There appears to be an effect due to the stalk in the bias coatings. The hemisphere opposite the stalk, where Fig. 18b was taken, appears to be relatively more smooth than the area immediately surrounding the stalk. This is not surprising since the stalk is part of the charging circuit, and the symmetry of the electric field lines near the stalk will be different from that opposite the stalk. Nevertheless, the effect of a bias voltage is to improve the coating smoothness at all locations. We have found similar results for Cu deposited on biased microballoons.

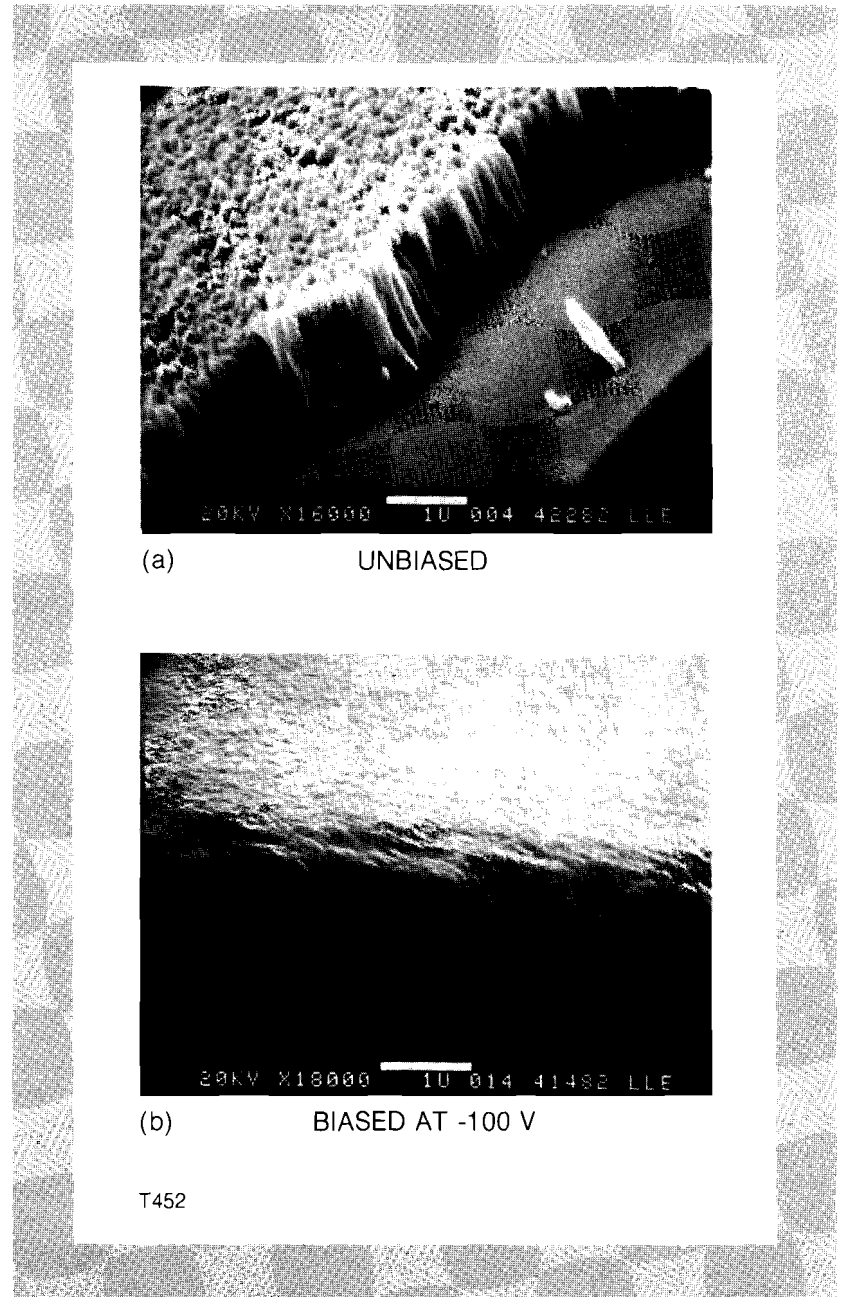


Fig. 18
Comparison of Ni coatings applied to a) un-biased and b) biased microballoons under otherwise identical conditions. The applied bias of -100V clearly results in a denser microstructure and smoother surface than that found in the unbiased coating.

Current work is directed at reducing the perturbation due to the stalk and studying the coating environment through the use of Langmuir probes. We feel that this method, based on experimental results to date, shows considerable promise for improving the microstructure, density, and surface smoothness of target pusher layers.

REFERENCES

1. S. F. Meyer, *J. Vac. Sci. Technol.* **18**, 1198 (1981).
2. R. W. Springer, B. L. Barthell, and D. Rohr, *J. Vac. Sci. Technol.* **17**, 437 (1980).
3. J. A. Thornton, *J. Vac. Sci. Technol.* **11**, 666 (1974).
4. D. M. Mattox and G. J. Kominiak, *J. Vac. Sci. Technol.* **9**, 528 (1971).
5. J. W. Patten, E. D. McClanahan, and J. W. Johnston, *J. Appl. Phys.* **42**, 4371 (1971).
6. D. W. Hoffman and M. R. Gaertner, *J. Vac. Sci. Technol.* **17**, 425 (1980).

3.B An Interactive Information Management Data Base for Fusion Target Fabrication

Multiple process steps are required to fabricate the targets used in irradiation experiments on the OMEGA laser system. Each step involves a measurement, layer deposition, gas fill, or assembly operation. A generic implosion target (see Fig. 19) is composed of four materials and requires more than a dozen processes in fabrication. These processes include:

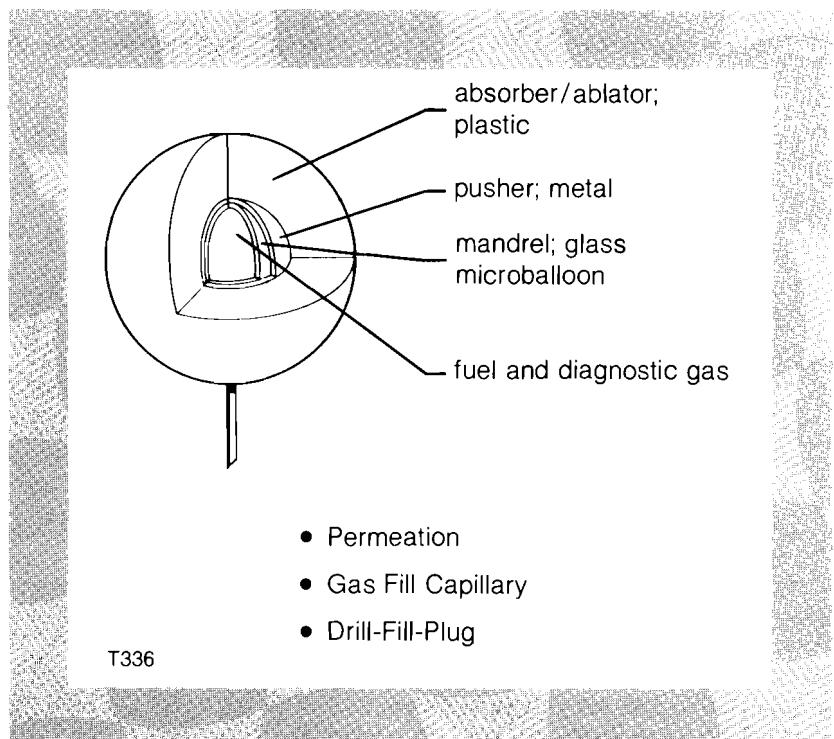
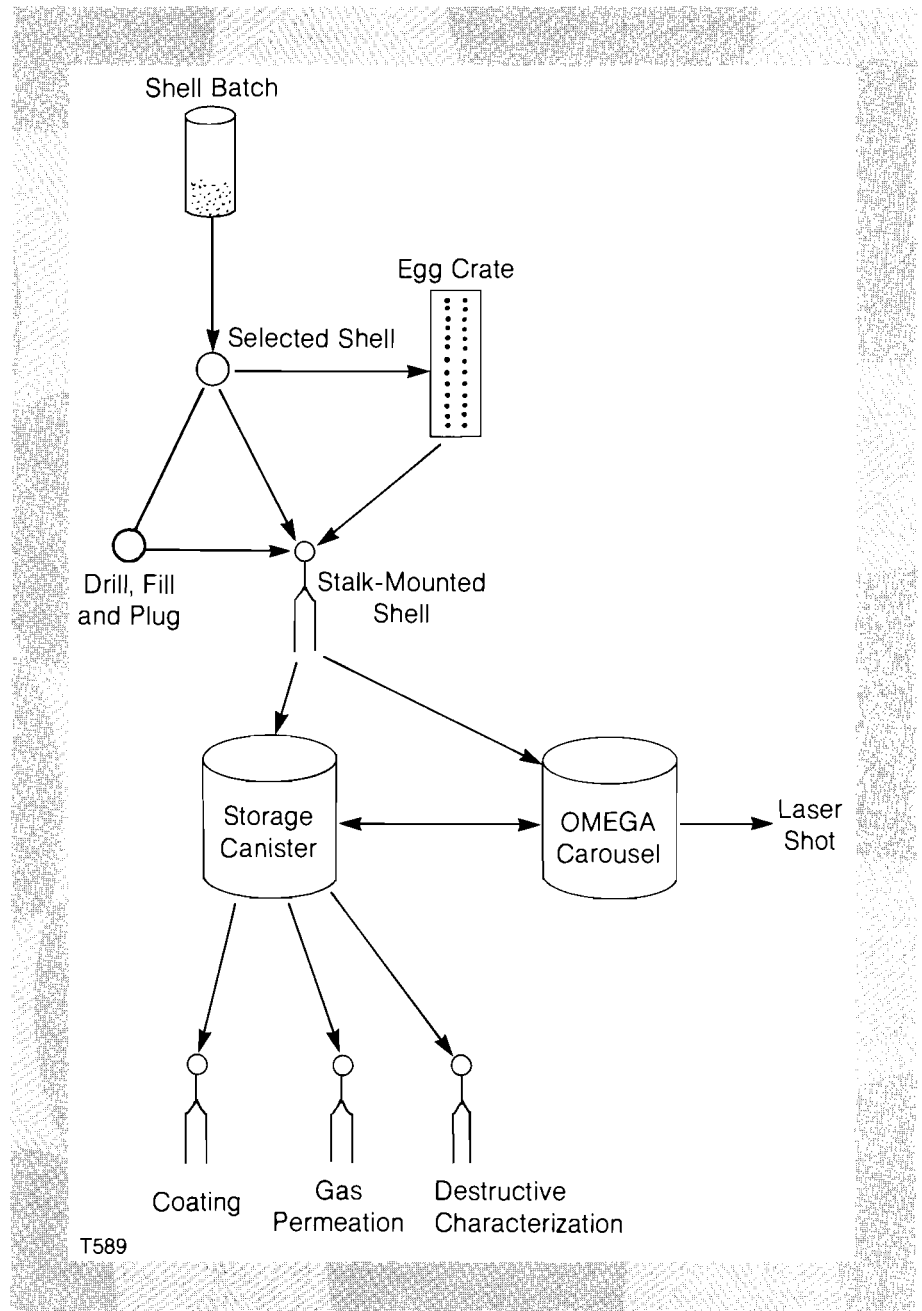


Fig. 19
Generic implosion target. The target consists of a GMB filled with a fuel gas and coated with layers of copper and plastic. The assembly is mounted on a glass stalk for positioning within the OMEGA target chamber.

- 1) glass microballoon (GMB) selection and characterization
- 2) fuel gas permeation and post-fill characterization
- 3) stalk mounting
- 4) copper layer deposition and characterization
- 5) plastic layer deposition and characterization

Each target has unique dimensions and specifications that are documented by measurements taken at each step of the fabrication process. More complicated types of targets are being made by the Target Fabrication Group which require different and/or additional process steps. Figure 20 shows some of the various paths a target may take during processing.

Fig. 20
Target fabrication process flowchart. A GMB may undergo various process steps and be stored in several different canisters before it is called for use on OMEGA.



T589

Records detailing each process step are necessary for an accurate description of the finished target. This record keeping becomes a sizable task given the thousand or more targets delivered by the Target Fabrication Group in a year, with large numbers of targets at various stages in the fabrication process at any given time. The need for detailed, accurate, and readily available data on the entire process has been met by the development of a computer-based information management data base.¹ The system provides:

- 1) automatic record storage
- 2) flexible data entry and computation
- 3) fast searching for targets with specific characteristics
- 4) automatic report writing
- 5) computerized transfer of information to other systems

The information management system resides on the Laser Computing Facility's CYBER 175 computer. The records are stored in indexed sequential files, which optimize the tasks of working on individual records and searching across the entire data base. Each target is assigned a unique identification number by the Target Fabrication Group when a specific target request is made; this number serves as the key for the target records.

There are four data files in the data base. The master file contains information on target location, as well as a summary of the more important physical parameters. There are three satellite files, which contain more specific information on the target layers, gases, and fuel-activity measurements. The satellite files also contain data on when a target record was entered into the data base, or modified, and by whom.

The data base was created so that the CDC data base language, Query Update,² could be used to read the data files. This is a unique use of a commercial data base language for handling scientific data. Query Update has many features that make it convenient for obtaining access to data from individual target records. However, its data entry procedures are inflexible and cumbersome to use in these circumstances. The need for more powerful, more flexible access to the data lead to the creation of front-end programs written in FORTRAN that can obtain access to the data files without recourse to Query Update (see Fig. 21).

Three types of front-end programs have been developed.

- 1) The Data Entry program is a menu-driven system that allows the users to create and update records in the data base as a process step is completed. The program collects raw data from the users and performs computations to determine the thickness of the various target layers, and the gas pressure of any targets containing tritium. It can also delete the records of targets that have been destroyed or lost.

- 2) The Report programs allow the users, both Target Fabrication Group members and OMEGA experimentalists, to obtain reports on desired targets. There is a short report that can display the major target parameters, and a master report that gives the entire target record. There is also a plotting package that allows the users to see the distribution of targets with regard to their physical parameters.

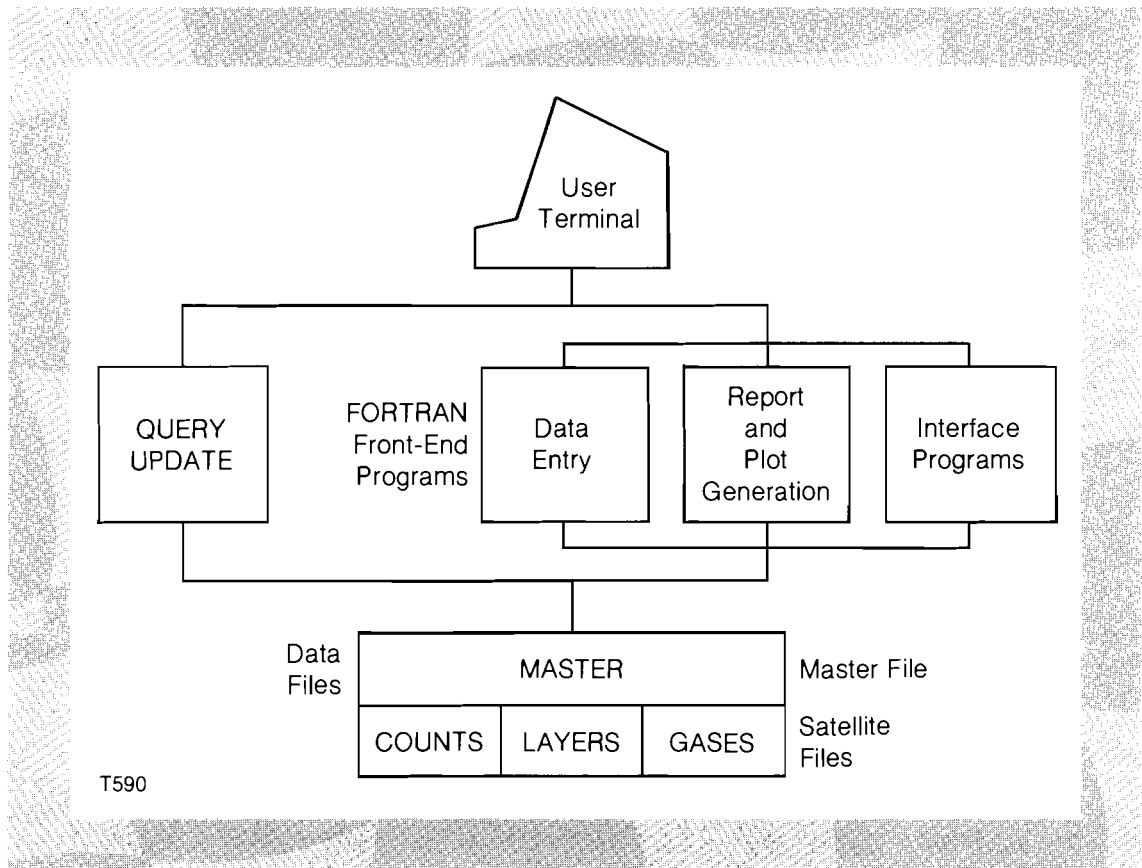


Fig. 21
Data base program schematic. The basis of the system is the data files; they can be accessed through Query Update or through the front-end programs.

3) There are other data bases in use at the LLE that rely on the data stored in the Target Fabrication Data Base; programs have been developed to automate the transfer of these data. When delivery of a set of targets in an OMEGA carousel is made, a program prepares individual target reports and a carousel summary report, updates the data base to note that the targets are now in a carousel, and creates a holding file that can be tapped by the OMEGA Laser System Data Base,³ and the OMEGA Experimental Data Base (see Fig. 22). The holding file contains the physical parameters of all the targets in the carousel, and some additional parameters such as target mass; information used only by the Target Fabrication Group, such as storage locations, is not transferred. The holding file is updated whenever new targets are loaded into an OMEGA target carousel.

When a target has been used by the OMEGA system, the data on the target are inserted into the Laser System Data Base and the Experimental Data Base. After the data have been preserved, the original records are deleted from the Target Fabrication Data Base automatically. The records can also be deleted by the Target Fabrication Group for targets that have been destroyed in testing, or lost.

The Target Fabrication Data Base thus performs several much-needed services for the LLE. The efficiency of the Target Fabrication Group personnel is augmented by the automation of tasks such as report writing. The data recorded are more reliable, since copying mistakes can be eliminated. The data are guarded from tampering, as a

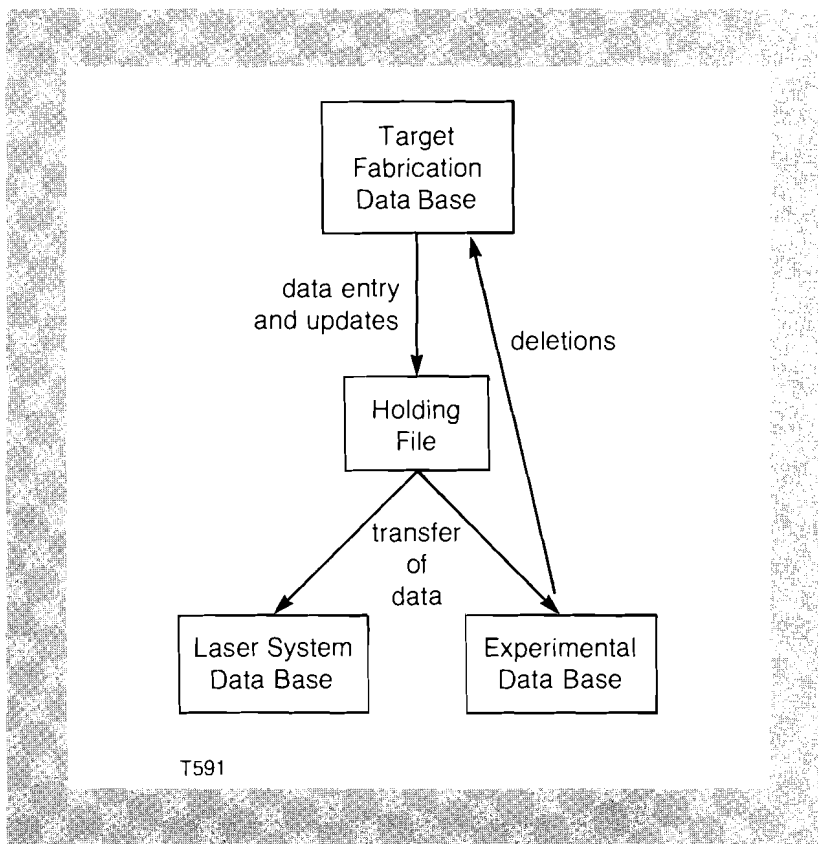


Fig. 22
Interface to other data bases. The target information in the holding file can be accessed by the Laser System Data Base, and by the Experimental Data Base. Once the information is transferred to the Experimental Data Base, the records are deleted from the Target Fabrication Data Base.

User Identification Code is required before the Data Entry program can be used. Information on target types, target components, and target parameters is made more accessible to the LLE as a whole through the searching and reporting mechanisms, and the interfaces to other LLE data bases. In summary, detailed, accurate, and readily available records of target fabrication are being efficiently handled by the computer-based information management data base.

REFERENCES

1. For information on the Target Fabrication Data Base, see the "Target Lab Data Base Entry and Report Programs", and the "CAROSEL Program" user manuals, available from the LLE.
2. Query Update Version 3 Reference Manual, Control Data Corporation Publication 60498300, Revision F (1980).
3. J. Boles, D. Pessel, L. Forsley, "OMEGA Automated Laser Control and Data Acquisition", *IEEE J. Quantum Electron.* QE-17, 1903 (1981).

Section 4

NATIONAL LASER USERS FACILITY NEWS

The National Laser Users Facility (NLUF) is currently hosting several user experiments. This report highlights the UCLA/Yale University, University of Maryland, and University of Illinois experiments. A brief summary of the completed Brigham Young University experiment is also included.

UCLA researchers Francis F. Chen, Chan Joshi, and Humberto Figueroa, in a joint effort with Yale University researchers Nizarali Ebrahim and Hiroshi Azechi, have obtained initial recordings of stimulated Raman spectra. They intend to measure the growth and angular dependence of stimulated Raman-scattered light and the angular dependence of electron spectra from an underdense plasma. The underdense plasma will be formed by focusing a $1.05 \mu\text{m}$ beam onto a thin foil which is then probed by a second pulse of $0.35 \mu\text{m}$ laser radiation. Measurements will be taken by two visible light spectrometers and two electron spectrometers to measure the Raman light and electrons produced from the plasma.

University of Maryland experimenters Hans Griem and John Adcock, in collaboration with Joe Reader from the National Bureau of Standards and Uri Feldman from the Naval Research Laboratory, are examining the Balmer Series spectra from low ions. An ultraviolet spectrometer, previously used in solar astronomy, has been installed on the GDL system to measure Balmer Series lines from various targets. To date, spectra have been observed from fluorine, graphite, plastic, iron,

niobium, and molybdenum. A full reduction of the data is being carried out at all three home institutions.

University of Illinois investigators George Miley, Aaron Bennish, Chan Choi, and Dave Harris are studying the energy losses of charged fusion products through the tamper (the hot outer-plasma region). A time-of-flight spectrometer, to measure the charged particles, has been installed on OMEGA. The spectrometer consists of two quadrupole magnets which relay the charged fusion products from the targets to a scintillator-photomultiplier. Transmission curves, indicating the fraction of charged fusion product collected at the spectrometer, have been generated.

Brigham Young University's Larry Knight, James Thorne, and David Gaines, working with Troy Barbee of Stanford University, are credited with the first user experiment completed at the NLUF. They developed new measurement techniques for x-ray radiation to probe high-density plasmas. These techniques involved the development of new x-ray optics using layered thin synthetic structures to supplement the more standard x-ray diffraction crystals.

The following is excerpted from the final BYU report:

A practical method of fabricating x-ray optics is crucial to the development of a system for the x-ray probing of dense plasmas. Layered Synthetic Microstructures (LSM's) appeared to have a real chance of filling this need. Relatively little x-ray characterization has been done on LSM's, at least as measured against their potential value. The Brigham Young University experiments performed low energy characterization of LSM's on the laser facility at BYU, followed by experiments at LLE. Experiments were conducted with both flat crystals and crystals bent in a cylindrical shape.

Two series of experiments were performed at the National Laser Users Facility; the first was of a preliminary nature in May 1981 and the second was just completed (August and September of 1981).

Direct comparison measurements were made between a tungsten/carbon LSM and a standard T.I.A.P. diffraction crystal on the GDL laser at LLE. Spectra were taken at 8 Å (aluminum) and at 15 Å (fluorine). Densitometer traces of the fluorine comparison spectra are shown in Fig. 23. The LSM had 150-layer pairs of tungsten/carbon with a total d-spacing of 15 Å. The LSM spectra have lower resolution and somewhat lower reflectivity than the T.I.A.P. spectra. The lower resolution was expected and the lower reflectivity is not surprising for an LSM with a small d-spacing. The fact that the spectra are comparable in these two respects is in itself an interesting result.

We consider the LSM's performance to be quite good. Its reflectivity is clearly reduced from that of an ideal structure. A defect-free LSM would have an integrated reflectivity about

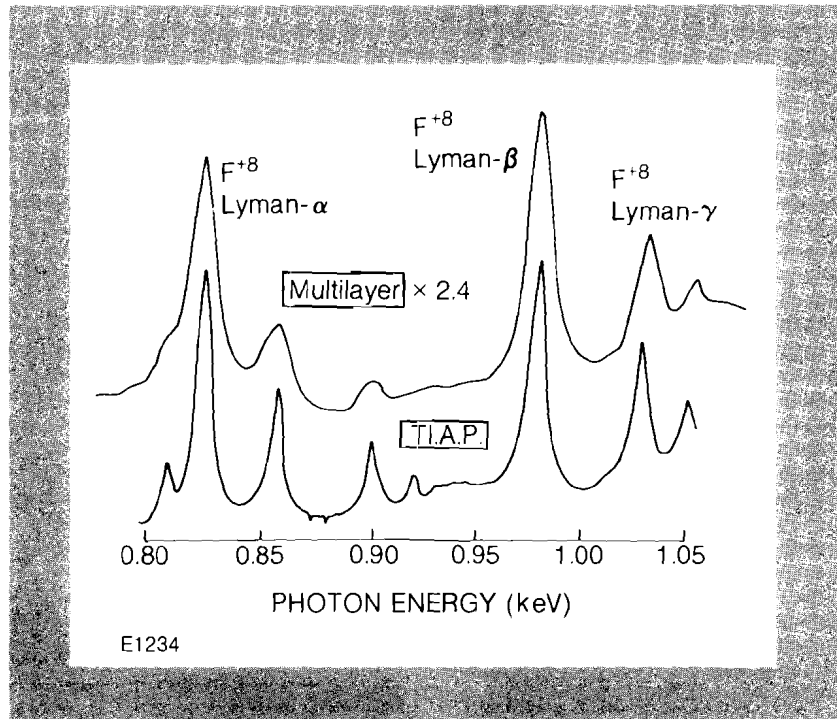


Fig. 23
Comparison of a fluorine x-ray spectra diffracted by a multi-layer and standard T.I.A.P. crystal. Scale of the upper trace increased by 2.4 over the lower trace.

60% greater and a peak reflectivity 40% lower than T.I.A.P. The reduced reflectivity of the real LSM is probably due to surface roughness effects.

(A copy of the entire report may be obtained from the National Technical Information Service, 5285 Port Royal Road, Springfield, Virginia 22161, \$8.00 per printed copy.)

Additional user experiments will be described in the next issue of the LLE Review. The users include Anthony J. Burek (National Bureau of Standards), Uri Feldman (Naval Research Laboratory), and Chuck Hooper (University of Florida).

Further information on the NLUF is available from:

Dr. Thomas C. Bristow, Manager
National Laser Users Facility
Laboratory for Laser Energetics
University of Rochester
250 East River Road
Rochester, New York 14623

PUBLICATIONS AND CONFERENCE PRESENTATIONS

Publications

W. Seka, R. S. Craxton, J. Delettrez, L. M. Goldman, R. Keck, R. L. McCrory, D. Shvarts, J. M. Soures, and R. Boni, "Measurements and Interpretation of the Absorption of 0.35 μm Laser Radiation on Planar Targets", *Opt. Commun.* **40** (6), 437-440 (1982).

G. Mourou and T. Sizer, "Generation of Pulses Shorter than 70 fs with a Synchronously-Pumped CW Dye Laser", *Opt. Commun.* **41** (1), 47-48 (1982).

Forthcoming Publications

G. F. Albrecht, "Temporal Shape Analysis of NA: YLiF Active Mode-locked/Q-Switched Oscillator", accepted for publication by *Optics Communications*.

D. Glocker and R. Wiseman, "A New Method for the Batch Production of Micro-Fresnel Zone Plates", accepted for publication by *Journal of Vacuum Science and Technology*.

D. A. Glocker, J. P. Drumheller, and J. R. Miller, "Ion Beam Sputter Deposition onto Levitated and Stalk-Mounted Laser Fusion Targets", accepted for publication by *Journal of Vacuum Science and Technology*.

T. F. Powers, "Improved Nonconcentricity Characterization of Trans-

parent Laser Fusion Targets by Interferometry", accepted for publication by *Journal of Vacuum Science and Technology*.

B. A. Brinker and J. R. Miller, "Capillary Gas-Filling of Inertial Fusion Targets", accepted for publication by *Journal of Vacuum Science and Technology*.

B. Yaakobi, J. Delettrez, L. M. Goldman, R. L. McCrory, W. Seka, and J. M. Soures, "Preheat Measurements in UV-Laser Target Interaction", accepted for publication by *Optics Communications*.

G. Mourou, W. Knox, and S. Williamson, "Picosecond High-Power Switching and Application", accepted for publication by *Laser Focus*.

K. Tanaka, L. M. Goldman, W. Seka, M. C. Richardson, J. M. Soures, and E. A. Williams, "Stimulated Raman Scattering from UV-Laser-Produced Plasmas", accepted for publication by *Physical Review Letters*.

G. Mourou and S. Williamson, "Picosecond Electron Diffraction", accepted for publication by *Applied Physics Letters*.

G. Mourou, W. Knox, and S. Williamson, "Advances in Picosecond Optoelectronics", accepted for publication by *S.P.I.E., Picosecond Lasers and Application*.

H. Kim, T. F. Powers, and J. Mason, "Real-Time Parylene Coating Thickness Measurement Using Optical Reflectometry", accepted for publication by *Journal of Vacuum Science Technology*.

S. Williamson, G. F. Albrecht, and G. Mourou, "Laser-Triggered Cr:GaAs HV Sparkgap with High Trigger", accepted for publication by *Review of Scientific Instruments*.

C. P. Verdon and R. L. McCrory, "Nonlinear Effects of Multifrequency Hydrodynamic Instabilities on Ablatively Accelerated Thin Shells", accepted for publication by *Physics of Fluids*.

S. Kacendar, S. Skupsky, A. Entenberg, L. M. Goldman, and M. C. Richardson, "Direct Measurement of the Fuel Density-Radius Product in Laser-Fusion Experiments", accepted for publication by *Physical Review Letters*.

Conference Presentations

R. E. Hopkins and M. Morris, "White Light Fourier Transform Lens", presented at Cuernavaca International Conference on Optical Instruments, Cuernavaca, Mexico, January 1982.

B. Yaakobi, "The Physics of Inertial Fusion", presented at the Latin-American Workshop on Plasma Physics and Controlled Nuclear Fusion Research, Cambuquira, Brazil, February 1982.

J. Forsyth and R. Frankel, "Nanosecond Exposure X-Ray Diffraction Patterns from Biological Specimens Using a Laser-Plasma Source", presented at the Biophysical Society Annual Meeting, Boston, Massachusetts, February 1982.

R. Frankel and J. Forsyth, "Time-Resolved X-Ray Diffraction Studies on

Purple Membrane from Halobacterium Halobium", presented at the Biophysical Society Meeting, Boston, Massachusetts, February 1982.

A. Simon, "Fusion Energy—Is It Coming?", presented at the American Society of Mechanical Engineers, Rochester, New York, February 1982.

Y. Conturie, B. Yaakobi, J. Delettrez, and J. Forsyth, "Soft X-Ray Population Inversions Observed in a Line-Focus Laser Plasma", presented at Laser Techniques for Extreme Ultraviolet Spectroscopy, Boulder, Colorado, March 1982.

R. Frankel, "Time-Resolved X-Ray and Optical Studies of Purple Membrane", presented at March Meeting of American Physical Society, Dallas, Texas, March 1982.

H. Kim and T. Powers, "Fabrication of Large-Aspect-Ratio Plastic-Coated Metal Shell Targets Using Leachable Polystyrene Mandrel", presented at Target Fabrication Specialists Meeting, Denver, Colorado, March 1982.

H. Kim, J. Mason, and J. R. Miller, "Ablation Layer Coating Using Alkylated DPX", presented at Target Fabrication Specialists Meeting, Denver, Colorado, March 1982.

J. R. Miller, "Overview of Laboratory for Laser Energetics Target Fabrication Program", presented at Target Fabrication Specialists Meeting, Denver, Colorado, March 1982.

This report was prepared as an account of work conducted by the Laboratory for Laser Energetics sponsored in part by the Empire State Electricity Energy Research Corporation (ESEERCO), the General Electric Company (GE), the New York State Energy Research and Development Authority (NYSERDA), Northeast Utilities (NU), the Standard Oil Company (Ohio) (SOHIO), the University of Rochester (U of R), and various governmental agencies. Neither ESEERCO, GE, NYSERDA, NU, SOHIO, DOE, the U of R, the government, nor their members or employees, nor any persons acting on their behalf either:

- a. Makes any warranty or representation, express or implied with respect to the accuracy, completeness, or usefulness of the information contained in this report, or the use of any information, apparatus, method, or process disclosed in this report may not infringe privately owned rights; or
- b. Assumes liability with respect to the use of, or for damages resulting from the use of, any information, apparatus, method or process disclosed in this report.

Reference herein to any specific commercial product, process, or service by trade name, mark, manufacturer, or otherwise, does not necessarily constitute or imply its endorsement, recommendation, or favoring by the United States Government or any agency thereof.

Results reported in the LLE Review should not be taken as necessarily final results as they represent ongoing research. The views and opinions of authors expressed herein do not necessarily state or reflect those of any of the above sponsoring entities.